

### Suggestions for revision

The revised version of the manuscript “Carbon mineralization in the Laptev and East Siberian Sea shelf and slope sediment” by Brüchert and co-workers was substantially improved in terms of structure and clarity in comparison to the original submission. The authors considered several of my comments but there are still several points that should be addressed before publication.

The assessment of the carbon burial efficiency (section 4.2) is still difficult to follow since the authors assumptions are not clearly described. The burial efficiency of terrestrial organic carbon seems to be derived from total carbon accumulation rates and sulfate reduction rates. But how is this possible if total organic carbon contains both marine and terrestrial carbon? From the authors response to my remarks to the original submission I understand that they assume that only marine organic matter decomposition is responsible for oxygen consumption. This is most likely not the case, as the authors are aware. This is yet a quite long paper and the authors might think about shortening the manuscript by omitting sections that are based on questionable assumptions.

Response: Section 4.2 has now been revised and shortened. We think that our analysis is qualitatively correct, but cannot be sufficiently resolved with respect to the oxic degradation of organic matter. We explain this in the text. Likewise the calculation of degradation constants suffers from our ability to resolve the terrestrial fraction of aerobically degraded material (although we think that this fraction is small compared to the marine fraction). We cannot infer directly how much of the oxygen uptake is due to terrestrial OM degradation. The reviewer’s comment refers to the old Boetius and Damm (1998) hypothesis, which is not sufficiently constrained. Based on our  $\delta^{13}\text{C}_{\text{DIC}}$  assessment, we know that terrestrial organic matter is remineralized anaerobically and there is no reason to assume that it is not degraded aerobically. However, the proportion of marine and terrestrial degraded by aerobic and anaerobic degradation likely differs, but we have no direct constraint to tell how much of the  $\text{O}_2$  uptake is due to terrestrial OM degradation alone, as sorry as we are about this conclusion ourselves.

The discussion still starts with the presentation of new results.

Response: This has been changed.

The numbering of the figures should be according to their reference in the text.

Done

The conclusion may substantially be shortened. Currently it is rather an extension of the discussion than a summary of the main findings of the presented work.

We shortened the text.

Specific comments:

Line 47ff: This statement is still not supported by the cited Hugelius et al. (2014) paper and the statement in the current form is still wrong. The authors should be aware of the difference between permafrost carbon (carbon in permafrost) and carbon in the permafrost region which comprises also carbon stored in non-permafrost deposits. According to Hugelius et al. (2014) 800 Pg C are stored in the permafrost, which is by definition frozen ground for more than 2 years. The phrase “perennially frozen permafrost” in the authors response is a tautology since permafrost is by definition perennially frozen. According to

Hugelius et al. (2014) about 500 Pg is stored in the permafrost region in seasonally or perennially unfrozen material (eg. active layer or river and lake sediments) which is not permafrost. The carbon in this non-permafrost pool contributes to the current carbon cycle and this carbon is the source for the terrestrial carbon in the investigated sediments. If the authors insist to refer to the number of 1100-1500 Pg given in the Hugelius paper they should refer to carbon in the permafrost region, as does the cited paper. The permafrost carbon pool, to which the authors still refer, is 500 Pg smaller, which is a significant number.

Response: We have now adapted the wording recommended by the reviewer and refer to the active layer carbon reservoir, with a remark to the currently frozen reservoir, part of which can thaw and oxidize in the future.

Line 56: Again, please clarify what is meant by “qualitative ... rates”. A rate is a quantitative measure.

Response: We removed the word qualitative

Line 175: DIC comprises beside dissolved CO<sub>2</sub> also bicarbonate and carbonate. Please clarify if only dissolved CO<sub>2</sub> was considered or total DIC.

Response: We replaced CO<sub>2</sub> with total dissolved inorganic carbon

Line 275: ... proportion of mineralized terrestrial...

Response: We changed the wording accordingly.

Line 345: The authors should comment on station 63 where the rates measured with the two methods deviate by a factor of 15.

Response: We discuss this in section 3.4 lines 414-418. Briefly, we observe very low rates of degradation in the buried sediments below 8 cm depth. At the same time, at this station the O<sub>2</sub> uptake was very high (>10 mmol m<sup>-2</sup> d<sup>-1</sup>). Since this is the easternmost station of our study and well under the influence of Pacific-derived nutrient water and given the enriched carbon isotope composition of the total organic matter, the marine carbon contribution here is very strong. It is therefore reasonable to assume that the present-day high O<sub>2</sub> uptake is due the mineralization of marine organic matter.

Line 366: The Fe concentration at 11 cm seems above 300µM, please clarify.

Response: The text refers to Station 30, where concentrations are lower and do not reach the concentrations mentioned by the reviewer. This only occurs further the east as is discussed in the following sentence.

Line 458ff: I suggest that these data should be presented in the results section with a reference to the respective figure before discussing them. The discussion should not start with the presentation of new results. Furthermore, the authors should give the statistical tests used for the correlation analysis. Since reduced sulfur oxidation is responsible for only a minor part of oxygen consumption, the authors might think about other reasons for

the observed correlation, e.g. burial of labile organic matter as discussed in lines 544-548.

**Response:** We have now moved this section to the results section.

Line 463: The slope of the regression line in Fig. 9 referred to in the preceding sentence is 5.5 not 6.1. It is unclear which “data set” is referred to here, since the authors presented a lot of interesting data. Please clarify. The regression analyses discussed here was not presented, and it’s difficult to follow the discussion of data that are not presented. Please clearly present data before they are discussed.

**Response:** We apologize for the confusion. As stated in the text, non-linear regression of all integrated sulfate reduction rates and oxygen uptake rates gave a slope of  $6.1 \pm 0.1$ . The depth-integrated sulfate reduction data are presented in section 3.3, lines 393-397 and Table 2 and then used further in the discussion by comparing them to the O<sub>2</sub> uptake rates (Table 2).

Line 513: Please explain DOC and POC

**Response:** Changed to dissolved organic carbon and particulate organic carbon

Line 523: Please explain BBL

**Response:** Changed to: benthic boundary layer

Lines 563. I still believe that the  $\delta^{13}\text{C}$  values of the bulk organic carbon of the investigated sediments are needed here to give the reader the chance to evaluate the modelled results presented by the authors. It is unclear to me why the authors refuse to present the bulk  $\delta^{13}\text{C}$  results so the reader can compare measured data with the results from the authors model. The authors state that they do not wish to reiterate published data in the discussion but to my opinion, an important aim of the discussion is to compare the presented data in the context of previously published data and the authors do so in other sections of the discussion. Knowing that lowest  $\delta^{13}\text{C}$ -values in the sediments of the investigation sites are at about -26‰ is important to evaluate the presented results. A  $\delta^{13}\text{C}$ -value of -35.8‰ for remineralized DIC is hardly explainable if no methane is involved (as the authors assume) and if the bulk organic carbon has values above -26‰. Hence, the authors might also include a sentence on the limitation of their modelling approach.

**Response:** There is a complete list of surface sediment concentrations for the investigated stations, including their isotope composition, and C/N ratios presented in Salvado et al (2017) Biogeosciences. We have added the referenced carbon isotope values to Table 1. A more detailed solid-phase composition data of a larger set of stations will be part of a separate publication.

By revising lines 460-470 (track changes) we have addressed the problem arising from the very light -35.8 value by assessing the range of uncertainty of our method, which is about 3 permil for the data from station 1. In addition, separating the DIC data of Station 1 into two sets – one for the top 20 cm and one for below that depth, yields a DIC endmember of -22.7 for the upper section and the measured light value of -35.8 for the bottom section. The light value of the bottom section possibly reflects the disappearance of the

most degradable marine organic matter in the topmost 20 cm of sediment. Figure 5B has been modified accordingly.

Lines 582 – 585: It is unclear how a  $\delta^{13}\text{C}$  value of -24‰ for marine organic matter is deduced from the reported Alling et al. (2012) values of -2 to -4 for the DIC. Has Alling et al. (2012) also measured  $\delta^{13}\text{C}$  values for the marine POC and which values did they find? Please clarify.

Response: In the past weeks a new publication on  $\delta^{13}\text{C}_{\text{POC}}$  in the Laptev and East Siberian Sea was published by Tesi et al (2017) Ocean Science. We have used values reported there for our end members in the Laptev Sea and East Siberian Sea and changed the reference and text of this section.

Lines 620-624: Could the authors please give the rates of Boetius and Damm (1988) here because most readers will not know them by heart.

Response: These rates are now included in the text and a statistical comparison was made with student's T-test.

Line 633: The authors might use statistical tests to test for significant differences between these datasets.

Response: We show the results of the student's T-test:

Line 635: East Siberian...

Response: Corrected

Lines 661 – 663: It is unclear to me how the burial efficiency of terrestrial organic carbon can be estimated by using the accumulation rates of total organic carbon comprised of both terrestrial and marine organic carbon. Please clarify. Furthermore, please explain why only sulfate-reduction was considered and not total anoxic degradation rates.

Lines 664 – 667: This assumption of the approach seems to be refuted by the oxygen consumption rates (see discussions in lines 688 – 694). Please clarify.

Line 667 – 668: Please explain why these numbers are substantially different than in the original manuscript ( $91\pm 6\%$  and  $94\pm 4\%$  in contrast to  $69\pm 28\%$  and  $79\pm 6\%$  in the original submission).

Response to last three comments: A significant fraction of iron and manganese reduction is directly coupled to reoxidation of sulfide produced by bacterial sulfate reduction. Simply adding the Fe and Mn reduction to the SRR gives a maximum estimate of anoxic carbon degradation. We have no good handle how much of the metal reduction is heterotrophic and how much is due to reoxidation of sulfide and can therefore only provide minimum and maximum estimates, respectively. Secondly, the degradation process rates all produce  $\text{CO}_2$ , but the isotope composition of the two reflects the mixture of oxidized terrestrial and marine organic carbon and the mass balance explained before allows one to estimate the proportion of terrestrial carbon degradation contributing to

CO<sub>2</sub> via the anaerobic processes. Based on the comments by the reviewer, we have 1 reconsidered the text. In light of the fact that it is recommended that we shorten the text of the manuscript and since it appears that the current calculations have shortcomings because they can only applied to the anaerobic section of the sediment, we have decided to leave out the section on carbon burial efficiency, even though that we think that our calculations are probably qualitatively correct. Including the calculation of a burial efficiency that would include the oxic part of the sediment would require too many assumptions on the accumulation of the terrestrial and marine organic matter proportions that we cannot resolve satisfyingly. It is therefore best to refrain from these calculations.

The revised calculation of a burial efficiency only refers to bulk carbon and does not distinguish the marine and terrestrial fraction. Since the Pb-210 Corg accumulation underestimates the true Corg accumulation, we are now adding the O<sub>2</sub> uptake to the Pb-210 Corg accumulation and calculate the burial efficiency from this sum. With this revised calculation, significantly lower values for burial efficiency result.

Line 731: The section numbering needs to be revised and there is no section 4.3  
Done

Line 759: The numbers given in the manuscript are above 90%.  
This whole section is now revised.

1128: Table 4

#### References:

Alling, V., Porcelli, D., Mörrh, C. M., Anderson, L. G., Sanchez-Garcia, L., Gustafsson, Ö., Andersson, P. S., and Humborg, C., 2012. Degradation of terrestrial organic carbon, primary production and out-gassing of CO<sub>2</sub> in the Laptev and East Siberian Seas as inferred from  $\delta^{13}\text{C}$  values of DIC, *Geochimica et Cosmochimica Acta*, 95, 143-159.

Hugelius, G., Strauss, J., Zubrzycki, S., Harden, J.W., Schuur, E.A.G., Ping, C.-L., Schirmer, L., Grosse, G., Michaelson, G.J., Koven, C.D., O'Donnell, J.A., Elberling, B., Mishra, U., Camill, P., Yu, Z., Palmtag, J., Kuhry, P., 2014. Estimated stocks of circumpolar permafrost carbon with quantified uncertainty ranges and identified data gaps. *Biogeosciences* 11, 6573-6593.

## Carbon mineralization in Laptev and East Siberian Sea shelf and slope sediment

Volker Brüchert<sup>1,3</sup>, Lisa Bröder<sup>2,3</sup>, Joanna E. Sawicka<sup>1,3</sup>, Tommaso Tesi<sup>2,3,5</sup>, Samantha P. Joye<sup>6</sup>, Xiaole Sun<sup>4,5</sup>, Igor P. Semiletov<sup>7,8,9</sup>, Vladimir A. Samarkin<sup>6</sup>

<sup>1</sup> Department of Geological Sciences, Stockholm University, Stockholm, Sweden

<sup>2</sup> Department of Environmental Sciences and Analytical Chemistry, Stockholm University, Stockholm, Sweden

<sup>3</sup> Bolin Centre for Climate Research, Stockholm University, Stockholm, Sweden

<sup>4</sup> Baltic Sea Research Center, Stockholm University, Stockholm, Sweden

<sup>5</sup> Institute of Marine Sciences – National Research Council, Bologna, Italy

<sup>6</sup> Department of Marine Sciences, University of Georgia, Athens, U.S.A.

<sup>7</sup> International Arctic Research Center, University Alaska Fairbanks, Fairbanks, USA

<sup>8</sup> Pacific Oceanological Institute, Russian Academy of Sciences, Vladivostok, Russia

<sup>9</sup> Tomsk National Research Politechnical University, Tomsk, Russia

**Abstract** The Siberian Arctic Sea shelf and slope is a key region for the degradation of terrestrial organic material transported from the organic carbon-rich permafrost regions of Siberia. We report on sediment carbon mineralization rates based on O<sub>2</sub> microelectrode profiling, intact sediment core incubations, <sup>35</sup>S-sulfate tracer experiments, porewater dissolved inorganic carbon (DIC),  $\delta^{13}\text{C}_{\text{DIC}}$ , and iron, manganese, and ammonium concentrations from 20 shelf and slope stations. This data set provides a spatial overview of sediment carbon mineralization rates and pathways over large parts of the outer Laptev and East Siberian Arctic shelf and slope and allowed us to assess degradation rates and efficiency of carbon burial in these sediments. Rates of oxygen uptake and iron and manganese reduction were comparable to temperate shelf and slope environments, but bacterial sulfate reduction rates were comparatively low. In the topmost 20 to 50 cm of sediment, aerobic carbon mineralization dominated degradation and comprised on average 84% of the depth-integrated carbon mineralization. Oxygen uptake rates and <sup>35</sup>S-sulfate reduction rates integrated over the topmost 30 cm of sediment were higher in the eastern East Siberian Sea shelf compared to the Laptev Sea shelf. DIC/NH<sub>4</sub><sup>+</sup> ratios in porewaters and the stable carbon isotope composition of remineralized DIC indicated that the degraded organic matter on the

Siberian shelf and slope was a mixture of marine and terrestrial organic matter. Based on dual end member calculations, the terrestrial organic carbon contribution varied between 32% and 36%, with a higher contribution in the Laptev Sea than in the East Siberian Sea. Extrapolation of the measured degradation rates using isotope end member apportionment over the outer shelf of the Laptev and East Siberian Sea suggests that about 16 Tg C per year are respired in the outer shelf sea floor sediment. Of the organic matter buried below the oxygen penetration depth, between 0.6 and 1.3 Tg C per year are degraded by anaerobic processes, with a terrestrial organic carbon contribution ranging between 0.3 and 0.5 Tg per year.

Key words: Carbon mineralization, Arctic shelf and slope sediment, Laptev Sea, East Siberian Sea

## 1. Introduction

The biogeochemical fate of terrestrial organic carbon deposited on the Arctic shelf and slope is one of the most important open questions for the marine Arctic carbon cycle (e.g., Tesi et al., 2014; Macdonald et al., 2015; McGuire et al., 2009; Vonk et al., 2012). The total pan-Arctic terrestrial permafrost ~~carbon~~ region has been estimated to contain about 1100 – 1500 Pg, of which 500 Pg are seasonally or perennially unfrozen and contribute to the present-day carbon cycle (Hugelius et al., 2014) ~~—a~~. Additional partial thawing, mobilization, and oxidation of the perennially frozen carbon ~~pool large enough to reservoir can~~ substantially affect the global atmospheric carbon dioxide pool over the next 100 years, ~~even when only partially decomposed after thawing and oxidation~~. (Schuur et al. 2015; Koven et al., 2015). ~~Yet, there remains~~ A key problem in this context is the considerable uncertainty regarding the mineralization of terrestrial organic matter exported by rivers and coastal erosion to the Siberian shelf and slope (Tesi et al., 2014; Karlsson et al. 2015; Semiletov et al., 2011; Salvado et al., 2016).

Terrestrial organic matter transported to the Siberian shelf is of variable size, age, and molecular composition, which results in a range of different carbon degradation rates of bulk carbon and individual molecular components. Size class analysis of the organic matter suggests that coarse organic material settles preferentially in near-shore environments, whereas finer organic fractions disperse offshore in repeated deposition-resuspension cycles gradually losing particular molecular components and overall reactivity (Wegner et al., 2013;

Tesi et al., 2014, 2016). Substantial oxic degradation of organic matter may occur during near-bottom transport in resuspension-deposition cycles across the shelf (Bröder et al., 2016a). Up to 90% of certain biomarker classes may decompose during transport, whereby most of the degradation may take place while the transported organic material resides in the sediment before being resuspended (Bröder et al., 2016a). However, without making approximations on transport direction, particle travel time and travel distance these studies cannot provide direct insights into the rates of carbon degradation and resultant CO<sub>2</sub> fluxes from sediment. By contrast, direct kinetic constraints provided by sediment carbon degradation rates can provide testable data for coupled hydrodynamic biogeochemical models that help assess the fate of land-exported terrestrial carbon pool on the Siberian shelf.

Relatively few studies have directly measured rates of carbon mineralization rates in Siberian shelf sediment (e.g., Boetius and Damm, 1998; Grebmeier et al., 2006; Karlsson et al., 2015, Savvichev et al., 2007). Boetius and Damm (1998) used high-resolution oxygen microelectrode data to determine the surface oxygen concentration gradients and oxygen penetration depths in a large number of sediment cores from the shelf and slope of the Laptev Sea. Based on corresponding sediment trap and export productivity data, they concluded that the annual marine organic carbon export in the Laptev Sea shelf and slope was sufficiently high to explain the observed oxygen uptake rates. Current understanding therefore holds that due to the long annual ice cover and low productivity on the eastern Siberian Arctic shelf and slope, only a small amount of marine organic carbon is exported and buried in Laptev and East Siberian Sea shelf sediment. The highly reactive fraction of fresh organic matter is thought to degrade in the surface sediment (Boetius and Damm, 1998). Consequently, anaerobic respiration in buried sediment has been thought to be negligible and to reflect the degradation of unreactive terrestrially derived carbon compounds. To our knowledge, with the exception of a recent study by Karlsson et al (2015) a more direct assessment of terrestrial carbon-derived mineralization rates in buried shelf and slope sediment has not been reported for the East Siberian Arctic Sea.

In this study, we present data from oxygen microelectrode profiling experiments, porewater data of dissolved inorganic carbon and its stable carbon isotope composition, and <sup>35</sup>S-sulfate reduction rate experiments along a shelf-slope transect near 125°E in the Laptev Sea. Samples were taken during the summer 2014 on the SWERUS-C3 expedition with the Swedish icebreaker Oden. We combined these data with porewater analyses of dissolved



ammonium, sulfate, iron, and manganese to assess the major carbon degradation pathways and rates across the extensive outer Laptev and Siberian shelf and slope.

## **2. Materials and methods**

### **2.1. Sample collection**

Samples were collected at 20 stations from 40 to 3146 m water depth in the western Laptev and East Siberian Sea (Fig. 1 and Table 1). In this study we only report on sampling sites that showed no methane gas plumes, acoustic anomalies in the water column, or sediment blankings indicative of rising gas. In areas of active ebullition from the seafloor as seen by video imagery and acoustic gas blankings in the water column, the biogeochemistry of sea floor processes such as bacterial sulfate reduction, DIC concentration and its carbon isotope composition, and oxygen uptake are affected by methane oxidation. These methane cycling-related signals overprint the biogeochemistry imparted by carbon mineralization and are reported in a separate study.

Sediment stations had variable ice cover (Table 1). In the Laptev Sea, except for the deep-water slope stations between 3146 m and 2106m, all stations had open water. By contrast, ice cover exceeded 75% in the East Siberian Sea to the west and east of Bennett island (Station 40 to 63). Sediments with well-preserved sediment surfaces were collected with a Multicorer (Oktopus GmbH, Kiel, Germany) that simultaneously takes 8 sediment cores over an area of about 0.36 m<sup>2</sup> with acrylic tubes (9.5 cm diameter, 60 cm length) to 40 cm depth preserving clear water on top of the sediment. At stations 6, 23, and 24, an underwater video system (Group B Distribution Inc., Jensen Beach, U.S.A.) was mounted on the multicore frame to record the deployment and recovery, and to document the sea floor habitat. For the investigations all cores were taken from the same cast. Two of the cores were used to determine <sup>35</sup>S-sulfate reduction rates and porosity. In addition, one core with predrilled 3.8 mm holes sealed with electric tape was used to extract porewaters with rhizons (Rhizosphere Research Products BV, Wageningen, Netherlands). A fourth core was used for microelectrode measurements of dissolved oxygen concentration profiling, and finally, four other cores were used for whole-core incubations to determine benthic fluxes of dissolved oxygen, dissolved inorganic carbon, and nutrients. The cores were capped with rubber stoppers until further subsampling usually within 30 minutes. For sulfate reduction rates, the

128 cores were subsampled with 40 or 50 cm long acrylic tubes (26 mm inner diameter) prepared  
129 with silicon-sealed holes, drilled at distances of 1 cm. For whole-core incubations, the cores  
130 were sub-sampled with 25 cm-long, 60 mm-wide tubes (56 mm id) to 12 cm depth. Likewise,  
131 a 60 mm diameter tube (56 mm id) was collected for microelectrode measurements preserving  
132 about 3 cm of the overlying bottom water. For intact whole-core incubations, temperature-  
133 controlled aquaria were filled with bottom water that was collected from a CTD rosette from  
134 the same station by collecting water from four ten-liter rosette bottles usually ~5 meters above  
135 the sea floor. All sediment cores were closed with a stopper retaining the water on top of the  
136 sediment and stored at 1.5°C in an incubator until further processing.

137

## 138 **2.2. Microelectrode oxygen profiles**

139 High-resolution O<sub>2</sub>-profiles across the water-sediment interface were obtained to  
140 determine oxygen penetration depths and diffusive oxygen uptake (Rasmussen and Jørgensen,  
141 1992; Glud, 2008) (Table 2). The 60 mm tubes were placed in an aquarium filled with bottom  
142 water from the same station, overflowing the sediment core. The water temperature was kept  
143 to ~1°C by a cooling unit (Julabo GmbH, Seelbach, Germany). In exceptional cases when  
144 there was not sufficient bottom water available to fill the aquarium, bottom water was used  
145 from a pump system. A stable diffusive boundary layer above the sediment was created by  
146 passing air from an aquarium pump over the water surface with a Pasteur pipette creating a  
147 slow rotational motion of water inside the core. At each station six to eight O<sub>2</sub> microprofiles  
148 were measured using Clark-type oxygen microelectrodes (OX-50, Unisense, Århus Denmark)  
149 mounted on a motor-driven micromanipulator (MM33, Unisense, Århus Denmark). O<sub>2</sub>  
150 sensors were calibrated with fully oxygenated bottom water from the same station at ~1°C for  
151 saturation and for anoxic conditions by dissolving Na<sub>2</sub>SO<sub>3</sub> in the same water. The first profile  
152 in each core was measured with a resolution of 1000µm as a quick scan to locate the sediment  
153 surface and to adjust the measuring range. Then the vertical resolution was increased to 100-  
154 500µm and additional five to seven profiles were measured at different points on the surface,  
155 approximately one cm apart from each other.

156

### 157 **2.3. Whole-core sediment incubations**

158 Four intact cores with clear overlying water were subsampled in the laboratory in  
159 acrylic tubes (i.d. 56 mm, height 25 cm) retaining about 10 cm of the overlying water. The  
160 sediment and water height in the tubes were approximately 10 cm. The cores were incubated  
161 in a 40-liter incubation tank filled with bottom water from the same station. Before the  
162 incubation the overlying water in the cores was equilibrated with bottom water in the tank.  
163 The overlying water in the cores was stirred by small magnetic bars mounted in the core liners  
164 and driven by an external magnet at 60 rpm. The cores were pre-incubated uncapped for 6  
165 hours and subsequently capped and incubated for a period of 6 to 24 hours depending on the  
166 initial oxygen concentration in the bottom water. 2D oxygen sensor spots (Firesting oxygen  
167 optode, PyroScience GmbH, Aachen, Germany) with a sensing surface of a diameter of 5 mm  
168 were attached to the inner wall of two incubation cores. The sensor spots were calibrated  
169 against O<sub>2</sub>-saturated bottom water and oxygen-free water following the manufacturer's  
170 guidelines accounting for temperature and salinity of the incubation water. Measurements  
171 were performed with a fiberoptic cable connected to the spot adapter fixed at the outer core  
172 liner wall at the spot position. The O<sub>2</sub> concentration was continuously logged during  
173 incubations. Sediment total oxygen uptake (TOU) rates were computed by linear regression of  
174 the O<sub>2</sub> concentration over time. 5 ml of overlying water were removed over the course of the  
175 incubation used for nutrient and dissolved CO<sub>2</sub> analysis as described below. Linear regression  
176 best fits were used to determine the exchange fluxes of dissolved CO<sub>2</sub>.

177

### 178 **2.4. Extracted porewater analysis**

179 Porewater samples for concentration measurements of total dissolved inorganic carbon  
180 (DIC), sulfate, and ammonium were obtained using the methods described in Seeberg-  
181 Elverfeldt et al. (2005). Rhizons were treated for 2 hours in 10% HCl solution, followed by two  
182 rinses with deionized water for 2 hours and final storage in deionized water. The rhizons were  
183 connected to 10 mL disposable plastic syringes with inert pistons (VWR, Stockholm, Sweden)  
184 via polyethylene 3-way luer-type stopcocks (Cole-Parmer, U.S.A.) and inserted in 1-cm  
185 intervals through tight-fitting, pre-drilled holes in the liner of the sediment cores. The first mL  
186 of pore water was discarded from the syringe. No more than 5 ml were collected from each core  
187 to prevent cross-contamination of adjacent porewater due to the suction effect (Seeberg-

Elverfeldt et al., 2005). The collected porewater was divided into four different aliquots for later chemical analysis. For dissolved sulfate analysis, 1 ml of porewater was preserved with 200  $\mu$ l of 5% zinc acetate solution and frozen. For ICP-AES analysis of dissolved metals and major cations, 1 ml of porewater was preserved with 100  $\mu$ l of 10% Suprapur  $\text{HNO}_3$  and stored cold. For analysis of dissolved ammonium, 2 ml of porewater were frozen untreated. For analysis of dissolved inorganic carbon, 2 ml of porewater were preserved with 100  $\mu$ l 10%  $\text{HgCl}_2$  and stored cold in brown glass vials without headspace. Ammonium was determined on a QUAATRO 4-channel flow injection analyzer (Seal Analytical) on board. All other porewater analyses were performed at the Department of Geological Sciences, Stockholm University. Samples that were analyzed in the home laboratory remained cold or frozen on board until arrival of the icebreaker Oden in Sweden. Sulfate concentration was measured on diluted aliquots on a Dionex System IC 20 ion chromatograph. DIC concentrations were determined by flow injection analysis (Hall and Aller, 1992). Dissolved iron and manganese were determined on diluted aliquots by ICP-AES (Varian Vista AX). For carbon isotope analysis of dissolved inorganic carbon, 1 ml of porewater was filled into 12 ml exetainers to which 1 ml of concentrated phosphoric acid was added. The carbon isotope composition of the formed  $\text{CO}_2$  was analyzed on a GasbenchII-MAT 253 isotope ratio mass spectrometer coupled to a GC-PAL autosampler. Results are reported in the conventional delta notation relative to PDB. Precision of isotope analysis is 0.1‰.

For the calculation of porewater concentration ratios of DIC and  $\text{NH}_4^+$ , the effects of different diffusion coefficients and ammonium adsorption were accounted for. We have no direct measurements of adsorption coefficients for these sediments. Instead, we used an ammonium adsorption coefficient of 1.3 established for comparable, terrestrially dominated silty clays in the East China Sea for which similar porosities and organic carbon concentrations were reported (Mackin and Aller, 1984). The diffusion coefficient of  $\text{HCO}_3^-$  is about 45% smaller than the diffusion coefficient of  $\text{NH}_4^+$  (Li and Gregory, 1974). The two effects required an upward correction of the ammonium concentration by 40% to facilitate direct comparison in DIC/ $\text{NH}_4^+$  ratios. Diffusion- and adsorption-adjusted DIC/ $\text{NH}_4^+$  ratios were also corrected for the bottom water DIC and  $\text{NH}_4^+$  concentrations (Table 1). Only concentrations below 4 cm depth were used for comparison to avoid effects of oxidation on  $\text{NH}_4^+$  concentrations.

## 2.5. Reaction transport modelling

Reaction rates and fluxes were estimated from the concentration profiles of dissolved oxygen, manganese, iron, and dissolved inorganic carbon according to the general reaction-transport equation at steady state accounting for diffusion and advection exemplified here for dissolved oxygen according to

$$\frac{d}{dz} = \left( \varphi(D_s + D_b) \frac{dO_2}{dz} \right) + \varphi \alpha (O_{2, z=0} - O_{2, z}) + \sum R = 0$$

(1)

At steady state, the rate of the concentration change reflects the balance between the consumption due to respiration and oxidation of reduced inorganic compounds (R) against diffusion and advection due to bioirrigation into sediment (Glud, 2008).  $D_s$  ( $\text{cm}^2 \text{s}^{-1}$ ) is the sediment diffusion coefficient and was calculated for the experimental temperature and salinity according to Boudreau (1997). The sediment diffusion coefficient  $D_s$  was recalculated from the molecular diffusion coefficient  $D_o$  according to  $D_s = D_o / \theta^2$ , where  $\theta^2 = 1 - \ln(\varphi^2)$ , where  $\varphi$  is porosity and  $\theta$  is tortuosity (Boudreau, 1997).  $D_b$  ( $\text{cm}^2 \text{s}^{-1}$ ) is the bioturbation coefficient and  $\alpha$  is the irrigation coefficient ( $\text{cm s}^{-1}$ ).  $D_b$  and  $\alpha$  were estimated by stepwise optimization by fitting a concentration profile to the measured data using the least square fitting procedure of the program Profile (Berg et al., 1998) testing various coefficients until the statistically best fit was obtained. Boundary conditions and the coefficients  $D_b$  and  $\alpha$  for the best fits are shown in the supplemental material Table 1.

## 2.6. $^{35}\text{S}$ -Sulfate reduction rates

For the incubations, the whole-core incubation method by Jørgensen (1978) was used.  $^{35}\text{SO}_4^{2-}$  tracer solution was diluted in a 6 % NaCl solution containing 0.5 mM  $\text{SO}_4^{2-}$  and 2.5  $\mu\text{l}$  of the tracer solution (200kBq) was injected through the pre-drilled holes. The cores were then capped and sealed in plastic wrap foil and incubated for 8 hours at the respective bottom water temperatures. After this time, the incubations were stopped by sectioning the core in 1-cm intervals to 5 cm depth and in two centimeter intervals below this depth to the bottom of the core. Sediment sections were transferred into 50 ml plastic centrifuge tubes containing 20 ml zinc acetate (20% v/v), mixed to a slurry on a vortex stirrer and frozen. The total amount of  $^{35}\text{S}$ -labeled reduced inorganic sulfur (TRIS) was determined using the single-step cold chromium distillation method by Kallmeyer et al. (2004). TRIS and supernatant sulfate were

counted on a TriCarb 2095 Perkin Elmer scintillation counter. The sulfate reduction rate was calculated using the following equation (Jørgensen, 1978):

$$^{35}\text{SRR} = \left( \text{TRI}^{35}\text{S} \times 1.045 / (^{35}\text{SO}_4^{2-} + \text{TRI}^{35}\text{S}) \right) \times [\text{SO}_4^{2-}] / \rho T \quad (2)$$

where  $[\text{SO}_4^{2-}]$  is the pore water sulfate concentration corrected for porosity  $\rho$ ,  $\text{TRI}^{35}\text{S}$  and  $^{35}\text{SO}_4^{2-}$  are the measured counts (cpm) of sulfate and total reduced inorganic sulfur species, respectively, 1.045 is a correction factor accounting for the kinetic isotope effect of  $^{35}\text{S}$  relative to  $^{32}\text{S}$ , and  $T$  is the incubation time. The sulfate reduction rate is reported as  $\text{nmol cm}^{-3} \text{ day}^{-1}$ .  $^{35}\text{SRR}$  were measured in two parallel cores for all depth intervals. The incubation experiments were conducted between July 15 and August 20, but for logistical reasons (transport to Stockholm) the distillation of the samples was conducted between December 10, 2014 and April 2, 2015 so that between 1.7 and 2.7 half-lives of  $^{35}\text{S}$  (87.4 days) had passed before all samples were processed. The resulting detection limit of the rate measurements accounting for distillation blanks and radioactive decay of  $^{35}\text{S}$  between experiment and laboratory workup was  $0.01 \text{ nmol cm}^{-3} \text{ day}^{-1}$ .

## 2.7. Carbon equivalent apportionment of terminal electron-accepting processes (TEAP)

The modelled oxygen, iron, manganese, and DIC reaction rates were integrated over a 30 cm sediment depth interval to permit comparison between different stations. The integrated terminal electron accepting processes (TEAP) rates were recalculated into carbon equivalents for the electron acceptors oxygen, iron, manganese, and sulfate using an idealized  $(\text{CH}_2\text{O})_x$  stoichiometry for organic matter (Vandieken et al., 2006; Nickel et al., 2008). The contribution of inorganic reoxidation to oxygen consumption and the effects of internal recycling of sulfur, iron, and manganese are discussed in section 4.1. The calculated rates were then used to calculate the contribution of the different aerobic and anaerobic electron acceptors to total carbon mineralization for 5 stations in the Laptev and East Siberian Sea (Table 3).

## 2.8 Marine versus terrestrial endmember partitioning of carbon degradation rates

279 In order to determine the proportion of mineralized terrestrial and marine organic  
 280 matter in the sediment directly, we used the DIC concentration and the carbon isotope  
 281 composition of DIC to determine the contribution of remineralized organic matter to  
 282 porewater DIC using a simple isotope mass balance model. Porewater DIC is assumed to be  
 283 derived from bottom-water DIC and remineralization of organic matter during burial. We  
 284 used a Keeling-type plot of  $1/DIC$  against the corresponding stable carbon isotope  
 285 composition of DIC to determine the isotope composition of the remineralized ~~end~~  
 286 ~~member~~endmember by linear regression. The method assumes that diffusion is slow  
 287 compared to burial and mineralization and that isotope fractionation during the oxidation of  
 288 organic matter is negligible. Removal or addition of DIC by diagenetic processes such as  
 289  $CaCO_3$  precipitation or dissolution were minor. This is supported by the observation that the  
 290 porewater concentrations of  $Ca^{2+}$  and  $Mg^{2+}$  at these shelf and slope stations did not change  
 291 significantly with depth (Brüchert and Sun, unpubl. data). The relative contribution of the  
 292 terrestrial and marine organic carbon was calculated with a linear two-endmember isotope  
 293 model:

$$294 \quad \delta^{13}C_{DIC, \text{remineralized}} = f_{terr} * \delta^{13}C_{terr \text{ OC}} + f_{mar} * \delta^{13}C_{marine \text{ OC}} \quad (4)$$

295 where  $f_{terr}$  and  $f_{mar}$  are the respective mass fractions of terrestrial and marine-derived organic  
 296 carbon and  $\delta^{13}C_{terr \text{ OC}}$  and  $\delta^{13}C_{marine \text{ OC}}$  reflect the isotope composition of these endmembers.  
 297 For the Laptev Sea shelf, a fraction of the surface water DIC used for marine production is  
 298 derived from terrestrial DOC and POC remineralized in shelf waters and transported from  
 299 land (Humborg et al., 2017; Tesi et al., 2017; Alling et al., 2012).  $\delta^{13}C$  values of offshore  
 300 sediment in the Laptev Sea sediment are as heavy as -22.3 ‰ (Salvado et al., 2016). Tesi et al  
 301 (2017) report  $\delta^{13}C$  of POC of -24.7 ‰ for outer Laptev Sea POC near the ice edge containing  
 302 abundant dinoflagellates and only trace indicators of terrestrial organic carbon. Based on these  
 303 data we use an isotope endmember composition of -23.0 ‰ for marine organic matter in the  
 304 Laptev Sea. We are aware that there may be regional variations in this endmember  
 305 composition. An isotope composition of -28 ‰ was used for the terrestrial organic carbon  
 306 contribution in the Laptev Sea (Vonk et al., 2012). For the East Siberian Sea east of 140°E,  
 307 the heaviest calculated isotope composition of remineralized porewater DIC was -19 ‰ and is  
 308 used here as the marine endmember (Station 53). The same carbon isotope composition of -28  
 309 ‰ as for the Laptev Sea was used as the terrestrial end member. In order to derive specific  
 310 degradation rates of the marine and terrestrial carbon fractions, the endmember mixing-based

311 assessment of the marine and terrestrial organic carbon contributions to DIC were combined  
312 with the mineralization rates derived for the different electron acceptors.

313

### 314 **3. Results**

#### 315 **3.1. Physical and chemical bottom water conditions**

316 Table 1 summarizes the general site characteristics of the investigated sediment  
317 stations. Bottom water salinity varied between 34.9 ‰ in the outer Laptev Sea at 3146 m  
318 depth (Station 1) to 29.1 ‰ in the East Siberian Sea at 40 m (Station 45). The lower salinity  
319 in the East Siberian Sea can be attributed to longshore transport of freshwater eastward from  
320 the Lena River. Bottom water temperatures varied between -1.8°C at Station 27 and 0°C at  
321 Station 37, but there was no regional trend in the data. Cored sediment consisted of silty clays  
322 to clayey silts. Slope sediment had a distinctly brown color throughout the cored interval,  
323 whereas shelf sediment only had a 1 to 4 cm-thick brown interval, below which the sediment  
324 color changed to grey. In the eastern part of the East Siberian Sea, the sediment was mottled  
325 black below 10 cm depth. Iron-manganese concretions were found between 2 cm and 10 cm  
326 depth at stations 24, 42, and 43, but were also observed at other stations on the shelf that were  
327 not part of this study. Benthic macrofauna, when present, consisted mainly of brittle stars,  
328 isopods, few polychaetes, and rare bivalves. All bottom waters were well-oxygenated with  
329 concentrations higher than 190 µmol/l, but the shelf bottom-waters in the East Siberian Sea  
330 had generally lower concentrations than in the Laptev Sea and bottom waters on the  
331 continental slope had lower oxygen concentrations than on the shelf. Concentrations of  
332 bottom-water ammonium ranged between 0.2 µmol/L and 1.8 µmol/L. Generally, the slope  
333 stations and the shelf stations nearest to the Lena delta had the highest ammonium  
334 concentrations, whereas the other shelf stations showed no clear regional trend other than  
335 proximity to the Lena delta. Bottom water dissolved inorganic carbon concentrations varied  
336 between 2086 µM (Station 53) and 2598 µM (Station 27), and the stable carbon isotope  
337 composition of DIC in the waters overlying the cores were between -0.5 ‰ and -6.5 ‰ vs.  
338 VPDB.

339

#### 340 **3.2. Dissolved oxygen, manganese, and iron**



We show representative profiles of oxygen concentrations in Figure 2 for the Laptev Sea slope station 1, the Laptev Sea shelf stations 23, 30, 45, and the East Siberian Shelf Sea 53 and 63. Oxygen penetration depths varied between 3 mm at Station 58 and more than 60 mm in all slope sediments (Table 2). For the Laptev Sea slope stations 1, 2, 3, and 4, the maximum depth of oxygen penetration could not be determined, because at penetration greater than 60 mm the conical sensor needle opened a hole in the sediment through which oxygen-containing bottom water could potentially have entered the sediment at depth thereby artificially extending the oxygen penetration depth. In the slope-to-shelf transects the oxygen penetration depth decreased from >60 mm off-shore to 10 mm at the most inshore station in the Laptev Sea and the East Siberian Sea. At the two easternmost shelf stations 58 and 63, we measured the lowest oxygen penetrations depths, 3 mm and 4 mm, respectively. Evidence for bioturbation and bioirrigation based on multiple microelectrode profile measurements per core was rare. Only at Station 48 a clear increase in oxygen concentrations below the sediment surface was observed, indicative of active bioirrigating macrofauna. However, even at this station, based on investigations in parallel multicore casts, fauna was not abundant (A. Gukov, pers. comm.). At all other stations, oxygen concentrations decreased exponentially with depth. Fitting of the oxygen concentration profiles to the steady advection-diffusion-transport model (Eq. 1) yielded fluxes that varied between 0.81 and 11.49 mmol m<sup>-2</sup> d<sup>-1</sup> (Table 2). These calculated O<sub>2</sub> fluxes compared well with total oxygen uptake rates calculated from whole-core incubations using 2D optode sensor spots (Table 2). The good fit between the two methods also supports the notion that bioirrigation and bioturbation effects from meiofauna and macrofauna were minor.

In the slope sediment at Station 1, concentrations of dissolved manganese and iron were low throughout the cored depth interval and below 0.2 and 0.5 µM, respectively. The exception was a small increase for both elements between 4 and 8 cm depth and 14 and 20 cm depth to concentrations of less than 3 µM, possibly due to slightly more degradable organic material in these depth intervals (Fig. 2). A similar concentration profile was found for the other slope station 4 (data not shown), but here concentrations were below 2 µM throughout for both dissolved iron and manganese and only slightly higher in the topmost cm. On the shelf, in the Laptev Sea (Station 23 and 30), concentrations of dissolved manganese and iron were below 0.3 µM and 1.5 µM, respectively, in the top 2 cm and 3 cm at Station 23, before increasing to maximum concentrations of 69 and 134 µM. At both stations, metal concentrations decreased again below the concentration maximum indicating that deeper

buried sediment was not a source of the metals and that the dominant source of iron and manganese was reduction in the topmost 5 cm of sediment. There was a general trend of increasing manganese concentrations from west to the east. At Station 30 in the Laptev Sea, the concentration of dissolved manganese was less than 0.3  $\mu\text{M}$  in the topmost cm, but increased steeply before increasing to maximum concentrations of 189  $\mu\text{M}$  at 9 cm depth. Similarly, dissolved iron concentrations were below 1  $\mu\text{M}$  to 4 cm depth and then increased to 144  $\mu\text{M}$ . Again, below the maximum, both iron and manganese porewater concentrations decreased with increasing sediment depth. Even higher iron and manganese concentrations were found in the East Siberian Sea (Stations 45, 53, 63), where dissolved manganese already increased from the bottom water to concentrations of 20  $\mu\text{M}$  in the topmost centimeter of sediment, and iron increased to above 1  $\mu\text{M}$  below 2 cm depth. The steepest manganese concentration gradient was found at Station 63 in the easternmost East Siberian Sea, where concentrations were 501  $\mu\text{M}$  in the first cm of sediment with a concentration maximum of 548  $\mu\text{M}$  at 2.5 cm depth and decreasing below this depth to 115  $\mu\text{M}$  at 30 cm depth. Station 63 differed with respect to dissolved iron concentrations from the other stations, because here dissolved iron showed two small peaks at 3.5 cm and 7 cm, and concentration increased substantially only below 17 cm depth to concentrations of 189  $\mu\text{M}$ .

### 3.3. $^{35}\text{S}$ -sulfate reduction rates and porewater sulfate

Sulfate concentrations showed minor depth gradients at all sampling sites (Fig. 3) and decreased from starting concentrations between 23.9 mM and 28.1 mM by 0.4 mM to 2.5 mM from the top to the bottom of the cores. At all stations, turnover of  $^{35}\text{S}$ -tracer was recorded from the topmost sediment interval to the bottom of the core indicating active bacterial sulfate reduction (Fig. 3). Depth-integrated rates over the recovered core lengths varied between 0.03 and 1.41  $\text{mmol m}^{-2} \text{d}^{-1}$  (Table 2). The integrated rates were lowest at Station 1 at 3146 m in the Laptev Sea and highest at the Station 63 in the easternmost East Siberian Sea. Across the shelf (Stations 6 to 24), depth-integrated rates increased from the west to the east. Example depth profiles of depth-specific sulfate reduction rates are shown in Fig. 3 for the same six stations as previously. At Station 1, these rates ranged from 0.03 to 0.38  $\text{nmol cm}^{-3} \text{d}^{-1}$ . At this station, the variability between replicate cores was large, which is attributed to the fact that many rates were near the detection limit in our handling procedure. Overall, sulfate reduction was higher in the top 10 cm of sediment, but showed no pronounced change with depth at this

station. This suggests that the reactivity of the organic material did not change substantially over the cored depth interval. The second slope station, Station 4, showed a similar rate-depth profile than Station 1. Depth profiles for the mid-outer shelf stations 23 to 63 all showed broad sub-surface maxima between 2.5 and 17.5 cm, but the depths of the rate maxima differed between the different stations (Fig. 3). Peak rates varied between 0.6 nmol cm<sup>-3</sup> d<sup>-1</sup> at Station 30 and 39 nmol cm<sup>-3</sup> d<sup>-1</sup> at Station 63. The second highest rate, 7.6 nmol cm<sup>-3</sup> d<sup>-1</sup>, was found at the station nearest to the Lena delta, Station 23. At all stations, sulfate reduction rates decreased from the maxima to rates below 1 nmol cm<sup>-3</sup> d<sup>-1</sup> or to below the detection limit at the bottom of the cores. A particularly sharp decrease in the sulfate reduction rate was observed between 8 and 9 cm at Station 63, where rates dropped from 8.5 to 0.1 nmol cm<sup>-3</sup> day<sup>-1</sup> over 1 cm depth. Since sulfate was abundant throughout the cored intervals, this order-of-magnitude decrease indicates substantial changes in the reactivity of buried organic matter. Although no abrupt change in grain size or organic carbon was observed in this core, it is likely that a historical change in organic sedimentation took place during deposition across this time interval.

#### 3.4. Porewater dissolved inorganic carbon (DIC), ammonium (NH<sub>4</sub><sup>+</sup>), and δ<sup>13</sup>C<sub>DIC</sub>

Porewater concentrations of dissolved inorganic carbon (DIC) and ammonium (NH<sub>4</sub><sup>+</sup>) increased with depth at all stations (Fig. 4). The increase of DIC was between 0.6 mM (Station 23) and 2.3 mM (Station 45) over the cored sediment depths and ammonium concentrations increased between 16.8 μM (Station 1) and 549 μM (Station 50). The steepness of the depth gradients was consistent with the rates of oxygen uptake and bacterial sulfate reduction for the different stations. The porewater pattern at Station 63 ~~is was~~ an exception, because this station had the highest oxygen uptake and the highest sulfate reduction rates of all stations, but showed only a modest increase in DIC and NH<sub>4</sub><sup>+</sup> concentrations by 1.5 mM and 57 μM, respectively, over the cored sediment depth. ~~This apparent discrepancy can be explained by~~ The low DIC concentrations are consistent with the very low rates of sulfate reduction below 10 cm depth. Since these deeper layers have not produced large amounts of DIC and NH<sub>4</sub><sup>+</sup>, only the surface 10 cm contribute significantly to total carbon mineralization and ammonium production.

For the anoxic parts of the sediment, DIC/NH<sub>4</sub><sup>+</sup> ratios varied between 8.4 for Station 24 and 40 respectively for Stations 1 in the Laptev Sea, and between 7.2 and 18.8 in the East Siberian

Sea, with an overall mean DIC/NH<sub>4</sub> ratio of 9.8 for all stations excluding the continental slope stations (Fig. 6a5a). The  $\delta^{13}\text{C}$  values of DIC consistently decreased with sediment depth indicating the addition of  $^{13}\text{C}$ -depleted remineralized carbon to DIC. The greatest downcore depletion in  $^{13}\text{C}$  was observed at stations 45, 48, and 50, where  $\delta^{13}\text{C}$  of DIC decreased from -2.0 ‰ near the sediment surface to -13.9, -16.4, and -18.6 ‰ at the bottom of the cores (Fig. 4).

Fig. 6b5b shows Keeling plots for the six stations presented before and Table 4 lists the derived carbon isotope compositions of remineralized organic matter for all stations. The range of  $\delta^{13}\text{C}$  of remineralized DIC varied between  $-18.8 \text{ ‰} \pm 1.1 \text{ ‰}$  (Station 53) and  $-35.8 \text{ ‰} \pm 3.0 \text{ ‰}$  in the lower part of Station 1. At this station, the data for the topmost 20 cm yielded an isotope composition of -22.7 ‰ for remineralized DIC. This isotopic composition reflects the bulk organic matter composition of sedimentary organic carbon at this station, which is -22.3 ‰ (Salvado et al (2016)). The more depleted values below 20 cm depth suggest that an isotopically distinct fraction of organic matter fuels carbon degradation in the buried sediments. ~~Terrestrially derived n-alkanes are known to have a  $^{13}\text{C}$ -depleted carbon isotope composition (Pagani et al., 2006) and~~ Salvado et al (2016) report terrestrial-derived lignin from sediment at this station- pointing to the presence of terrestrial organic matter. Terrestrially derived n-alkanes can have such low  $\delta^{13}\text{C}$  values (Pagani et al., 2006). Slow degradation of terrestrially derived lipids in these sediments suggests a contribution of terrestrial organic matter to carbon mineralization far offshore, in line with the very high DIC/NH<sub>4</sub><sup>+</sup> ratio of the porewaters at the slope stations. The contribution of degradable terrestrial organic matter to DIC in lower slope sediments is also supported by the observation of terrestrially derived biomarkers in porewater DOC of central Arctic Ocean sediment analyzed by FT-ICRMS (Rossel et al., 2016) and deep-water sediment trap data in the central Arctic Ocean (Fahl and Nöthig, 2007), but requires further investigation.

The calculated mass fractions of the marine and terrestrial endmembers are listed in Table 4. In the Laptev Sea on average 4847 % of the remineralized DIC is derived from terrestrial organic carbon. This proportion decreases to an average value of 3032% in the East Siberian Sea, in line with a greater marine production in this area due to the inflow of Pacific water (Semiletov et al., 2005; Dudarev et al., 2006; Naidu et al., 2000).

### 3.5. ~~Modelled~~ Benthic exchange and modelled oxygen, iron, and manganese reduction rates

Benthic exchange fluxes from whole-core incubations and modelled DIC fluxes are shown in Table 2. A good agreement was found between 2D oxygen optode flux measurements and the modelled O<sub>2</sub> concentration fluxes, whereas the modelled DIC fluxes were generally lower than the whole-core incubation fluxes. We attribute this discrepancy to an underestimation of the DIC gradient at the sediment-water interface. A representative result of the reaction transport modelling for dissolved oxygen, iron, and manganese is shown for Station 23 in Fig. ~~56~~. Optimal fits of the concentration profiles required a bioirrigation coefficient of  $1 \times 10^{-4} \text{ cm}^2 \text{ sec}^{-1}$  in the topmost 2 cm of sediment at Stations 23 and 53. For the other stations, optimal fits required no sediment mixing by bioturbation or advective porewater transport by bioirrigation. This is consistent with the low numbers of bioturbating macrofauna in the outer shelf sediment. O<sub>2</sub> consumption rates exceeded sulfate and net reduction rates of iron and manganese by a factor of ~~more than an order of magnitude~~ 100 (Fig. ~~56~~). On the shelf, most of the carbon oxidation therefore takes place in the topmost 5 mm. The reaction rate depth profiles for iron and manganese ~~reduction~~ indicate that manganese reduction dominates in the topmost 2 cm of sediment followed by co-existing iron and sulfate reduction below (Fig. ~~56~~). Bacterial sulfate reduction was already detected at a depth where the sediment was still brown indicating abundant iron and manganese ~~oxyhydroxides~~ hydroxides. Coexistence of net iron reduction and sulfate reduction at the same depths make it difficult to quantify how much of the iron reduction is coupled to heterotrophic carbon oxidation and to the re-oxidation of sulfide produced from bacterial sulfate reduction. Qualitatively, the presence of dissolved iron throughout the measured porewater profile implies that iron reduction exceeded concomitant sulfate reduction, iron sulfide precipitation, and reoxidation reactions, which supports the assessment of net heterotrophic iron reduction. However, previous investigations of the importance of iron and manganese reduction in Arctic shelf sediments have emphasized the importance of ~~directly~~ coupled redox processes between iron and manganese and sulfide (Vandieken et al., 2006). It is also important to note that iron and manganese oxyhydroxides can sorb  $\text{Mn}^{2+}$  and  $\text{Fe}^{2+}$  (Canfield et al. 1993). The concentrations of dissolved  $\text{Fe}^{2+}$  and  $\text{Mn}^{2+}$  may therefore underestimate the actual concentrations of the reduced forms in these sediments. Assuming no direct redox coupling between the terminal electron-accepting processes, manganese and iron reduction contributed maximally between 2.3 and 23.7% to the total anaerobic carbon

Formatted: Indent: First line: 1.27 cm

mineralization and between 0.3 and 2.3% to the total carbon mineralization (Table 3). Even if these numbers overestimate the contribution of metals to carbon mineralization, the results indicate that bacterial sulfate reduction is by far the major anaerobic carbon mineralization pathway in these sediments. The prevalence of bacterial sulfate reduction in anaerobic carbon mineralization agrees with results of Vandieken et al. (2006) and Nickel et al. (2008) from the northern Barents Sea ~~that more~~where ice-free stations supported higher rates of sulfate reduction than the more permanently ice-covered stations reflecting lower carbon export production.

The modelled negative iron production rates at the sediment surface indicate net iron oxidation by oxygen in the mixed upper sediment layer. This pattern was not observed for manganese, which is consistent with incomplete manganese oxidation at the sediment surface and loss of dissolved manganese to the bottom water. The efflux of manganese to the bottom water on the eastern Siberian shelf supports results by Macdonald and Gobeil (2012) that Arctic shelves can export dissolved manganese to the Arctic interior. Consistent with these observations there was a statistically significant positive correlation between the dissolved oxygen uptake and anaerobic carbon degradation rates by sulfate reduction ( $r^2$  0.~~7275~~,  $P < 0.05$ ) (Fig. 7). This reflects the coupling of oxygen uptake to the oxidation of reduced inorganic metabolites (FeS and H<sub>2</sub>S) produced during sulfate reduction (e.g., Glud, 2008; Jørgensen and Kasten, 2006; Thamdrup, 2000; Berg et al., 2003) ~~(Fig. 9)~~. The slope of the regression line for all stations ~~is at which sulfate reduction rates were determined was~~  $6.1 \pm 1.1$  ~~indicating that. The percentage of~~ the inverse of this slope, ~~about~~ 16.4% ~~of %, reflects~~ the ~~oxygen uptake, is used for the average~~ oxidation of reduced manganese, ammonium, dissolved iron, iron sulfides, and elemental sulfur by oxygen. This amount is slightly lower than the average 23% estimated for oxygenated coastal and continental shelf sediment (Canfield et al., 2005), but is consistent with the notion that a substantial amount of the buried organic matter in Siberian shelf sediment is oxidized anaerobically. The lower proportion of anaerobic respiration to aerobic respiration compared to other shelf environments likely reflects the greater proportion of highly reactive marine-derived organic material in the topmost millimeters of sediment.

## 4. Discussion

### 4.1. Marine versus terrestrial organic matter contribution

Terrestrial organic carbon sources to the Laptev and East Siberian shelf and slope are riverine discharge and coastal erosion of the ice core complex (Stein and Macdonald, 2004; Vonk et al., 2012; Rachold et al., 2004; Fahl and Nöthig, 2007; Semiletov, 1999). Marine organic carbon is derived from open-water production during the ice-free months, export of ice algae, and new production in polynyas (Sakshaug et al., 2004; Nitishinsky et al. 2007). Generally, marine productivity in the Laptev Sea is low and controlled by the nutrient concentrations derived from Atlantic water, but spring outflow from the Lena River provides an additional temporary land-derived nutrient source (Pivovarov et al., 1999; Sakshaug et al., 2004; Nitishinsky et al., 2007; Bourgeois et al., 2017) during late spring ice melt (Raymond et al., 2007). Terrestrial-derived nutrients can also affect marine productivity either directly by new production, or indirectly, due to plankton production from remineralized terrestrial dissolved organic carbon and particulate organic carbon (Alling et al., 2012; Tesi et al., 2017). In the eastern East Siberian and Chukchi Sea, the inflow of nutrient-rich Pacific water supports higher marine primary productivity (e.g., Grebmeier et al., 2006). Ice-rafted transport and bottom boundary layer transport are the two most important modes of particle transport (Wegner et al., 2005; Bauch et al., 2009). Since all sediments sampled in this study were fine-grained silty clays and clayey silts, coarse-grained woody, ice-rafted material plays only a minor role for deposition of organic matter on the outer shelf and slope sediment. The transport direction of inner shelf sediments has been suggested to follow the predominant atmospheric regime, which is thought to be linked to the Arctic Oscillation (AO) (Dimitrenko et al., 2008; Guay et al., 2001; Weingartner et al., 1999). During positive AO southwesterly winds lead to generally eastward transport and repeated inshore transport in the benthic boundary layer, whereas negative AO favors southerly winds and a predominantly northward transport (Guay et al., 2001; Dimitrenko et al., 2008). Offshore transport of dissolved and particulate organic matter from the Lena delta to the north can occur with the Transpolar Drift, but terrestrial organic material is also transported eastward and obliquely offshore with the Siberian coastal current receiving additional organic material from the Indigirka and Kolyma rivers (Guo et al., 2007; Dudarev et al., 2006). East of 140°E, the influence of Pacific-derived nutrient-rich water supporting marine production is stronger the further east and offshore the sampling stations are located (Semiletov et al., 2005) (Fig. 1).

Carbon degradation rates in the sediment across the whole Siberian shelf and slope reflect this temporally and spatially diverse distribution of nutrient availability, ice cover, sediment deposition, and current flow regime (Rachold et al., 2004; Dudarev et al., 2006;

Semiletov et al., 2005; Sakshaug et al., 2004; Dmitrenko et al., 2005). The proportion of degradable marine-derived organic material at the eastern Stations 50 to 63 on the East Siberian shelf is higher than at the western stations in the Laptev Sea, in line with higher nutrient availability due to the Pacific influence. Ice-free conditions and the opening of water due to northward migration of ice shortly before the sampling likely supported new algal primary production at the shelf stations closest to land leading to enhanced export and deposition on the seafloor. During the time of sampling, only Stations 6 to 27 were ice-free, while Stations 23 and 24 had the longest ice-free condition before sampling. By contrast, Stations 30 to 63 were covered by ice during sampling. New export of reactive organic material explains why O<sub>2</sub> uptake rates were the highest at stations 23 and 24 along the shelf to slope transect from station 1 to station 24 (Boetius and Damm, 1998). The same pattern as for the O<sub>2</sub> uptake rates is also observed for the sulfate reduction rates indicating that reactive organic matter is also buried below the oxygen penetration depth and mixed sediment layer into the sulfate-reducing zone. This indicates that a greater portion of reactive organic material is buried closer to the Lena delta.

Published organic carbon budgets for the Arctic shelves infer an average burial efficiency of about 1% of exported marine OC (Stein and Macdonald, 2004), while terrestrial organic carbon, only accounting for about 10% of the organic carbon delivered to the Arctic Ocean bottom, has been suggested to be preserved with about 90% efficiency (Macdonald et al., 2015). Semiletov et al. (2016) compiled a large dataset indicating substantial aragonite undersaturation of Arctic shelf bottom waters from the Laptev, the East Siberian, and the Russian part of the Chukchi Sea and inferred widespread remineralization of terrestrial organic matter in the bottom waters and sediments. The observation of strongest aragonite undersaturation in the bottom waters supports a sediment-derived CO<sub>2</sub> source or a stagnant bottom boundary layer (Semiletov et al., 2013). It is therefore possible that oxic carbon mineralization in the topmost mm of sediment is a major CO<sub>2</sub> source for the overlying water.

Since <sup>35</sup>S-sulfate reduction rates comprise most of the anaerobic carbon mineralization of sediment buried below the oxygen penetration depth, our assessment includes, in contrast to earlier studies, ~~the mineralization rates~~an assessment of terrestrial organic matter mineralization beyond the short time period of oxygen exposure in the topmost mm of sediment. Using sedimentation rates of 0.8 mm y<sup>-1</sup> for the outer Laptev Sea (Strobl et al., 1988) and 1.4 mm y<sup>-1</sup> for the outer East Siberian Sea (Bröder et al., 2016b), the recovered sediments record a time interval of 250 to 700 years since burial. Using the mass fractions of



terrestrial and marine-derived organic carbon listed in Table 4, respective mineralization rates of the terrestrial and marine carbon fractions were calculated from the product of the mass fractions and the depth-integrated anaerobic carbon mineralization rates ~~(from Table 2).~~ This approach is only applicable ~~in~~ for depth-integrated anaerobic carbon mineralization rates and ~~cannot used to include the~~ is not possible without making assumptions for oxic carbon mineralization. ~~The reason for this is that the~~ depth of oxygen penetration varied only between a few millimeters to little more than a centimeter on the shelf, whereas the corresponding DIC concentration profiles, from which the marine and terrestrial proportions were derived, are affected by diffusive exchange along the 30 cm-long concentration profile. It is therefore not possible to assess the relative fractions of terrestrial and marine organic matter mineralized for discrete depth intervals ~~and/or~~ the oxic zone. ~~Our~~ Nevertheless, our combined radiotracer and DIC stable isotope approach suggests that both marine and terrestrial organic matter are degraded in the buried ~~sediment and that both pools contribute to degradation products in~~ buried sediment. This assessment is a significant modification to earlier studies by Boetius and Damm (1998) and Bourgeois et al. (2017), who have described organic matter mineralization in Siberian Arctic sediments largely as a function of oxygen uptake.

Carbon mineralization rates measured along the transect near 130°E (Stations 1 through 24) reflect the influence of gradual offshore transport of terrestrial organic material (Bröder et al., 2016a) (Fig. ~~7A8A~~, B). ~~A comparison with the oxygen~~ Oxygen uptake rates reported by Boetius and Damm (1998) ~~that measured in the early fall of 1993~~ ranged between 0.16 and 1.56 mmol m<sup>-2</sup> d<sup>-1</sup>. The data range in our study (0.81 to 11.49 mmol m<sup>-2</sup> d<sup>-1</sup>) covers the same water depth range and indicates that all rates measured in 2014 were significantly higher than the rates measured in 1993 by Boetius and Damm (1998). ~~Although~~ (Student's t-Test <0.01, one-tailed distribution, heteroscedastic). To some extent the different rates may reflect a seasonal effect ~~since, because~~ Boetius and Damm's data were acquired later in the year than our data. However, the increase may also point to higher organic carbon mass accumulation rates compared to 20 years ago, consistent with a decrease in the annual ice cover over the past 20 years in the Arctic (Arrigo and van Dijken, 2011; Stroeve et al., 2012; Walsh et al., 2017). Whether these rates reflect higher marine and/or terrestrial accumulation cannot be answered satisfyingly with this data set.

Fig. ~~8A9A~~ compares the oxygen uptake rate of the stations of this study with averaged oxygen uptake rates from the literature for different shelf, slope, and abyssal plain environments worldwide (Canfield et al., 2005). The data suggest that there is no significant

difference in the oxygen consumption rates between the Siberian shelf and slope and other continental margin environments. ~~(Student's T-test >0.5, one-tailed distribution, heteroscedastic).~~ <sup>35</sup>S-sulfate reduction rates in ~~Seathese East~~ Siberian slope ~~sediment~~ sediments are also comparable rates to those in other slope environments (Fig. ~~7B and 8B, 9B~~), but the sulfate reduction rates on the shelf are lower by a factor up to 15. Another difference apparent from this comparison is the similarity in sulfate reduction rates for the outer shelf and continental slope sediments of the Siberian Arctic (Fig. ~~8B, 9B~~). This similarity ~~is noteworthy for several reasons: 1) it~~ suggests that the kinetics of anaerobic carbon degradation in the shelf and slope sediments reflect similar reactivity of the organic matter. This is surprising since accumulation rates on the continental slope are probably significantly slower than on the outer shelf. 2) The absolute magnitude of the sulfate reduction rates in shelf and slope sediment indicate significant rates of organic matter mineralization long after burial consistent with the substantial DIC flux and the strongly <sup>13</sup>C-depleted DIC carbon isotope composition. Overall, the data indicate that organic matter reactivity substantially changes during burial in shelf sediment, but that the reactivity of transported organic matter that is exported to deep water across the shelf does not decrease significantly supporting further long-term slow mineralization rates in the slope environment. Accumulation of the organic material on the slope may therefore be related to rapid downslope transport of organic material or a rapid offshore transport, e.g., due to transport with ice or as bottom nepheloid layers cascading from the shelf edge (Ivanov and Golovin, 2007).

#### 4.2. Assessment of carbon burial efficiency

Reported <sup>210</sup>Pb-based sediment accumulation rates in outer Siberian shelf sediment range between 0.05±0.02 g cm<sup>-2</sup> y<sup>-1</sup> in the Laptev Sea (Strobl et al., 1988) and 0.24±0.04 g cm<sup>-2</sup> y<sup>-1</sup> in the East Siberian Sea (Bröder et al., 2016b). Given surface sediment organic carbon ~~concentration~~ concentrations for this area between 1% and 1.5%, the resulting organic carbon mass accumulation rates vary between 1.1 mmol m<sup>-2</sup> d<sup>-1</sup> and 1.7 mmol m<sup>-2</sup> d<sup>-1</sup> for the Laptev Sea (area near Station 23) and ~~5.5 and 8.2 mmol m<sup>-2</sup> d<sup>-1</sup> in the East Siberian Sea (data for Station 63).~~ We estimated the burial efficiency of terrestrial organic carbon from the ratio of the depth-integrated sulfate reduction rates relative to the <sup>210</sup>Pb mass accumulation rate of organic carbon. This treatment assumes that the reported organic carbon mass accumulation rates largely reflect the refractory component of organic matter. While it is possible that a

fraction of terrestrial and marine organic matter is degraded on shorter time scales than captured by the  $^{210}\text{Pb}$  method, we assume that the fraction of highly reactive terrestrial organic matter missed in this treatment is small. The resulting burial efficiency of the terrestrial carbon fraction is on average  $91 \pm 6\%$  in the Laptev Sea and  $94 \pm 4\%$  for the East Siberian Sea. We also calculated apparent degradation rate constants of organic matter assuming first order degradation kinetics for the time duration of sediment burial recorded in the sediment cores. For this assessment, we used the total depth integrated anaerobic carbon mineralization determined from the combined manganese, iron, and sulfate reduction rates for the recovered sediment. The apparent annual degradation rate constant ( $k$ ) was then calculated from

$$k_{\text{terrestrial}} = \frac{\left( -\ln \frac{\int_0^{30} \text{OC}_{\text{accumulation}} - \int_0^{30} \text{OC}_{\text{total mineralization}}}{\int_0^{30} \text{OC}_{\text{accumulation}}} \right)}{t_{\text{burial}}} \quad (5)$$

where the integrals of  $\text{OC}_{\text{accumulation}}$  and  $\text{OC}_{\text{mineralization}}$  cover a period of 250 years to 700 years based on the  $^{210}\text{Pb}$  mass accumulation rates. The resulting annual degradation rate constant ( $k_{\text{terrestrial}}$ ) ranges between  $1 \times 10^{-4} \text{ y}^{-1}$  and  $5 \times 10^{-4} \text{ y}^{-1}$  averaging  $1.5 \times 10^{-4} \text{ y}^{-1}$  in the Laptev Sea and between  $8 \times 10^{-5}$  and  $3 \times 10^{-4} \text{ y}^{-1}$  averaging  $1.2 \times 10^{-4} \text{ y}^{-1}$  in the East Siberian Sea.

between  $5.5$  and  $8.2 \text{ mmol m}^{-2} \text{ d}^{-1}$  in the East Siberian Sea (data for Station 63). A comparison of the total oxygen uptake with the  $\text{C}_{\text{org}}$  mass accumulation rates indicates that the  $^{210}\text{Pb}$ -based  $\text{C}_{\text{org}}$  mass accumulation rates on the shelf are equal or significantly lower than the oxygen uptake rates, with a discrepancy of up to a factor 10. Since the derivation of the  $^{210}\text{Pb}$ -based  $\text{C}_{\text{org}}$  mass accumulation rates is based on the same depth range as our direct  $^{35}\text{S}$ -based degradation rate measurements (30 cm of sediment, Vonk et al., 2012),  $\text{C}_{\text{org}}$  mass accumulation rates and anaerobic degradation rate measurements cover the same time window of sediment burial. Temporal variation in sediment accumulation therefore cannot explain the discrepancy. In addition, methane seep sediments where upward transport of methane from deeper sediment layers contributed to oxygen uptake were excluded from this data set. The best explanation for the discrepancy is therefore that the  $^{210}\text{Pb}$  mass accumulation rates underestimate the true mass accumulation rate of highly reactive organic material and that this material is oxidized at the sediment surface. The best explanation is that the  $^{210}\text{Pb}$ -mass accumulation rates underestimate the true  $\text{C}_{\text{org}}$  mass accumulation rate. Labile organic carbon is oxidized at the sediment surface and not adequately accounted for in the  $\text{C}_{\text{org}}$  measurements, likely due to coarse sediment sampling resolution. A better account of the true mass accumulation of organic carbon is therefore the sum of the oxygen uptake converted to

CO<sub>2</sub> equivalents plus the <sup>210</sup>Pb-based C<sub>org</sub> mass accumulation. ~~Based on the measured oxygen uptake rates this freshly deposited organic material has substantially higher degradation rates within the top mm of sediment as reflected by the steep O<sub>2</sub> gradients. <sup>210</sup>Pb-based organic carbon accumulation therefore reflects the long-term burial of less reactive organic material in the top 30 cm of sediment. Since anaerobic degradation processes prevail below the O<sub>2</sub> penetration depth, the measured burial efficiency of the accumulating organic material is therefore a function of the anaerobic bacterial degradation rather than the aerobic degradation efficiency. This conclusion has implications regarding the assessment of potential aerobic degradation of reactive terrestrial organic matter, since degradation of such material would have gone undetected with <sup>210</sup>Pb-based accumulation rate measurements.~~

We estimated the total burial efficiency of organic carbon from the sum of the depth-integrated aerobic and anaerobic degradation relative to the sum of the CO<sub>2</sub> equivalent from O<sub>2</sub> uptake and the <sup>210</sup>Pb mass accumulation rate of organic carbon. The resulting burial efficiency of the total organic carbon is on average 28 ± 10 % in the Laptev Sea and 52 ± 11 % for the East Siberian Sea. Based on the measured oxygen uptake rates this freshly deposited organic material has substantially higher degradation rates within the top mm of sediment as reflected by the steep O<sub>2</sub> gradients.

It is likely that this labile fraction consists of both terrestrial and marine organic matter, but the degradation kinetics of these two pools cannot be assessed reliably.

#### **4.53. Regional estimates**

We present areal estimates of sediment carbon mineralization by extrapolating the measured carbon mineralization rates over the outer Laptev Sea and East Siberian Sea shelf. Such extrapolations of benthic carbon mineralization rates are notoriously difficult given sediment heterogeneity and insufficient temporal data coverage of benthic carbon mineralization rates. For this investigation, no near-shore or slope stations were included in the assessment. The near-shore Siberian shelf environments are under much stronger influence by coastal erosion and riverine discharge than the outer shelf stations and have considerable longer open-water conditions than the outer shelf stations investigated here. In addition, the sedimentation pattern in the near-shore environments is significantly more

diverse, which will affect sedimentation rates, grain size distribution, and carbon contents. For this reason, we did not extend our extrapolations to the inner shelf environments. Some of these inner shelf settings likely have much higher benthic carbon mineralization rates and additional studies are required to constrain these better. Our coverage of the slope stations is insufficient for meaningful spatial extrapolations. ~~A large data set for this region has been analyzed by Miller et al. (2016) and the reader is referred to this work.~~

We estimate the extent of the outer shelf area with depositional conditions comparable to those investigated here to cover approximately 280,000 km<sup>2</sup> of the Laptev Sea. For the East Siberian Sea, we estimate the respective area of the outer shelf to be 340,000 km<sup>2</sup>. Due to the stronger terrestrial influence in the Laptev Sea, we calculated rates separately for the two shelf seas. The areal coverage with sediment stations was too sparse for statistically significant interpolations between stations that would give reliable spatial accounts of the gradients in rates between the stations. Instead, arithmetic averages of sediment mineralization rates and fluxes were calculated for these regions. Accepting the uncertainties in our assessment and data density, we estimate that the calculated areal rates could deviate by up to 50%. Table 5 lists the calculated rates based on the average flux calculated per square meter per day for oxygen uptake, DIC flux, bacterial sulfate, and total anaerobic carbon mineralization. For the latter three methods, the total flux was calculated for the marine and terrestrial component, respectively. The same analysis ~~cannot~~could not be performed for the oxygen uptake for the reasons discussed in section 4.3. Since the major part of the oxygen uptake is likely associated with degradation of a highly reactive marine organic carbon component, the proportions calculated based on the  $\delta^{13}\text{C}$  composition of DIC would not necessarily apply to the topmost mm of sediment. It is noteworthy to say that the rates calculated with our data set agree well with the O<sub>2</sub> uptake rates recently published by Bourgeois et al. (2017) for the Laptev Sea. Our calculations suggest that 5.2 and 10.4 Tg O<sub>2</sub> y<sup>-1</sup>, respectively are taken up by the outer shelf sediment in the Laptev and East Siberian Sea, respectively, totaling 15.9 Tg y<sup>-1</sup> for the whole investigated area (Table 5). Anaerobic carbon mineralization based on DIC, <sup>35</sup>S-SRR and combined manganese, iron, and sulfate reduction range between 0.62 and 1.28 Tg y<sup>-1</sup>. Of the total anaerobic carbon mineralization, between 0.25 and 0.48 Tg y<sup>-1</sup> can be attributed to the oxidation of terrestrially derived organic material. This rate is five to ten times lower than the estimated annual water column degradation of particulate terrestrial organic matter in the Eastern Siberian Arctic shelf system of 2.5±1.6 Tg y<sup>-1</sup> (Sanchez et al. 2011), and only

between 0.5% and 2% of the annual organic carbon export from land (Stein and Macdonald, 2004; Vonk et al., 2012).

## 5. Conclusions

Directly measured carbon mineralization rates together with stable isotope and concentration data of East Siberian Arctic shelf and slope porewaters indicate that about one third of the remineralized organic carbon in porewater DIC is derived from terrestrial organic matter. This conclusion confirms and extends previous observations that terrestrial organic carbon buried in Siberian shelf and slope sediment is not conservative (Semiletov et al., 2013; Karlsson et al., 2015; Bröder et al., 2016b). While mineralization of terrestrial organic material ~~has been was~~ described for the water column and resuspended surface sediment, our data indicate that mineralization also proceeds long after burial in sediment. ~~The estimated apparent carbon degradation rate constants of transformed terrestrial organic matter on the outer shelf are slow ( $< 3 \times 10^{-4} \text{ y}^{-1}$ ) and the overall terrestrial carbon burial efficiency is relatively high ( $> 87 \%$ ) and only slightly lower than previously reported based on millennial-scale carbon burial rates ( $> 90 \%$ , Stein and Macdonald, 2004).~~ Area-integrated rates of carbon mineralization in the outer shelf sediments (~~0.2925~~ to  $0.48 \text{ Tg y}^{-1}$ ) represent about 0.5 % to 8 % of the annual terrestrial organic matter load to the Laptev and East Siberian Sea ranging from  $6 \text{ Tg y}^{-1}$  (Stein and Macdonald, 2004) to  $22 \pm 8$  to  $44 \text{ Tg y}^{-1}$  (Vonk et al., 2012). There are large uncertainties associated with these estimates, given that our calculations do not account for carbon mineralization of resuspended terrestrial organic material and likely higher rates of mineralization in the inner shelf sediments. Nevertheless, these data indicate that the contribution of the benthic DIC flux to the total  $\text{CO}_2$  production in the outer Eastern Siberian Sea and Laptev Sea is small. This conclusion, however, does not necessarily extend to the inner parts of the Laptev Sea and the western parts of the East Siberian Sea, where  $\text{CO}_2$  supersaturation has been reported by Semiletov et al. (2012) and Pipko et al. (2011). Anderson et al (2009) estimated a DIC excess of  $10 \text{ Tg C}$  by evaluating data from the Laptev and East Siberian Seas collected in the summer of 2008 and suggested that this excess was caused mainly by terrestrial organic matter decomposition. Their estimate can be compared to our sediment oxygen uptake for the outer Laptev and East Siberian Sea shelf of almost  $16 \text{ Tg y}^{-1}$ , which would demand that 62.5 % of the oxygen uptake was due to terrestrial organic matter mineralization. However, the reported annual production of marine

791 organic matter for the total Laptev and East Siberian Sea is about 46 Tg y<sup>-1</sup> (Stein and  
792 Macdonald, 2004). Even if only half of this amount is produced in the outer shelf region and  
793 only another half of that amount was deposited, there would still be more than 10 Tg y<sup>-1</sup> of  
794 reactive marine organic matter at the sediment surface. Our data would therefore suggest that  
795 at least in the more productive East Siberian Sea the pronounced aragonite undersaturation  
796 reported for bottom waters in the East Siberian Sea is due to aerobic mineralization of a  
797 significant amount of marine organic matter, ~~which extends the assessment for the western~~  
798 ~~Chukchi Sea and the central Arctic Ocean by Qi et al. (2017).~~ It is apparent that these  
799 sediments play a major role in the recycling of marine organic carbon on the Arctic shelf.  
800 Future changes in marine production on the Siberian shelf under longer ice-free conditions  
801 (Arrigo and van Dijken, 2011) will likely change the relative proportions of degrading marine  
802 and terrestrial organic matter further so that this particular shelf system may in the future  
803 more strongly resemble that of other ice-free shelf-slope environments.

804

## 805 6. Acknowledgements

806 Funding for this investigation came from the K&A Wallenberg foundation, the Swedish  
807 Polarsekretariat, and the Bolin Centre for Climate Research at Stockholm University. Igor  
808 Semiletov acknowledge support from ~~the Russian Government~~ (No.  
809 14.Z50.31.0012/03.19.2014). We would like to thank the members of the SWERUS-C3  
810 consortium, the shipcrew on icebreaker Oden, and Heike Siegmund, Lina Hansson, Barkas  
811 Charalampos, and Dimitra Panagiotopoulou for help with the laboratory work. We dedicate  
812 this publication to our friend and colleague Vladimir Samarkin, who unfortunately passed  
813 away before publication of this work. This manuscript benefitted from discussions with  
814 Patrick Crill, Rienk Smittenberg, Örjan Gustafsson, Christoph Humborg, Julia Steinbach,  
815 Clint Miller, Marc Geibel, Emma Karlsson, Brett Thornton, Jorien Vonk, Leif Anderson, and  
816 Magnus Mörrth.

817

818

Formatted: Font: Not Bold

819 **List of Tables**

820

821 ~~Table 1. Physical and chemical characteristics of sediment and bottom water chemical~~  
822 ~~characteristics at the sampled stations.~~

823 ~~Table 2. Summary of oxygen penetration depth, O<sub>2</sub> uptake, and integrated <sup>35</sup>S sulfate~~  
824 ~~reduction rates.~~

825 ~~Table 3. Anaerobic rates of carbon mineralization by manganese, iron, and sulfate reduction~~

826 ~~Table 4. Calculated carbon isotope composition of remineralized DIC and mass fractions of~~  
827 ~~the marine and terrestrial end member and corresponding terrestrial carbon degradation rates~~  
828 ~~based on <sup>35</sup>S-SRR and DIC~~

829 ~~Table 5. Regional estimates of sediment carbon mineralization in the outer Laptev and East~~  
830 ~~Siberian shelf sea~~



**List of figures**

**Figure 1:** General map of the Laptev and East Siberian Sea with sediment stations and major current features

**Figure 2:** Depth profiles of dissolved  $O_2$  measured with  $O_2$  microelectrode sensors for Stations 1, 23, 30, 45, 58, and 63 and profiles of porewater concentrations of dissolved iron and manganese

**Figure 3:**  $^{25}S$  SRR rates and corresponding porewater sulfate concentrations for Stations 1, 23, 30, 45, 58, and 63

**Figure 4:** Depth profiles of dissolved inorganic carbon (DIC),  $\delta^{13}C_{DIC}$ , and dissolved ammonium ( $NH_4^+$ ) for Stations 1, 23, 30, 45, 58, and 63

**Fig. 5:** Comparison of reaction rates of oxygen, manganese, iron, and sulfate reduction at Station 23. Note the different depth scale for the  $O_2$  consumption rate. The dashed line marks the oxygen penetration depth

**Fig. 5 A, B:** Map of field area and sampling stations showing oxygen uptake rates in panel A and depth-integrated sulfate reduction rates in panel B. For comparison, oxygen uptake rates reported in Boetius and Damm (1998) using the same color coding are shown as triangles for comparison

**Fig. 6 A:** Crossplot of dissolved  $NH_4^+$  and porewater DIC\* after correction for bottom water DIC concentrations. The slopes of the regression lines for the individual stations are shown in Table 2. **B:** Crossplot of the fraction of remineralized DIC calculated from a two-endmember mixing

Formatted: Font: +Body (Calibri), 11 pt

model versus  $\delta^{13}\text{C}_{\text{DIC}}$ . The slope and y intercept of the regression for each station are shown in Table 3.

Fig. 7A, B. Map of field area and sampling stations showing oxygen uptake rates in panel A and depth integrated sulfate reduction rates in panel B.

Fig. 8A. Water depth variation of sediment oxygen uptake. 8B: Water depth variation of integrated  $^{35}\text{S}$  sulfate reduction rates (0-30 cm sediment depth). For reference average rates of abyssal plain, continental rise, slope, and shelf sediments, deposition and non-depositional, are shown for reference.

Fig. 9. Crossplot of diffusive oxygen uptake and integrated sulfate reduction rates. The black line is the linear regression and yielded a y intercept of  $2.1 \text{ mmol m}^{-2} \text{ d}^{-1}$  and a slope of 5.55. Blue and red lines show the 95% and 99% confidence interval.

Formatted: Font: +Body (Calibri), 11 pt

Formatted: Indent: First line: 1.27 cm

873 **7. References**

874

875 Alling, V., Sanchez-Garcia, L., Porcelli, D., Pugach, S., Vonk, J. E., van Dongen, B., Mörrh,  
876 C.-M., Anderson, L. G., Sokolov, A., Andersson, P., Humborg, C., Semiletov, I., and  
877 Gustafsson, Ö.: Non-conservative behavior of dissolved organic carbon across the Laptev and  
878 East Siberian seas, *Global Biogeochemical Cycles*, 24, 10.1029/2010gb003834, 2010.

879 Alling, V., Porcelli, D., Mörrh, C. M., Anderson, L. G., Sanchez-Garcia, L., Gustafsson, Ö.,  
880 Andersson, P. S., and Humborg, C.: Degradation of terrestrial organic carbon, primary  
881 production and out-gassing of CO<sub>2</sub> in the Laptev and East Siberian Seas as inferred from δ<sup>13</sup>C  
882 values of DIC, *Geochimica et Cosmochimica Acta*, 95, 143-159, 2012.

883 Anderson LG, Jutterström S, Hjalmarsson S, Wahlstrom I, Semiletov IP. Out-gassing of CO<sub>2</sub>  
884 from Siberian Shelf seas by terrestrial organic matter decomposition. *Geophysical Research*  
885 *Letters*, **36**, L20601, 2009.

886 Arrigo, K. R., and van Dijken, G. L.: Secular trends in Arctic Ocean net primary production,  
887 *Journal of Geophysical Research: Oceans*, 116, 10.1029/2011JC007151, 2011.

888 Bauch, D., Dmitrenko, I., Kirillov, S., Wegner, C., Hölemann, J., Pivovarov, S., Timokhov,  
889 L., and Kassens, H.: Eurasian Arctic shelf hydrography: Exchange and residence time of  
890 southern Laptev Sea waters, *Continental Shelf Research*, 29, 1815-1820, 2009.

891 Berg, P., Petersen-Risgaard, N., and Rysgaard, S.: Interpretation and measured concentration  
892 profiles in sediment pore water, *Limnology and Oceanography*, 43, 1500-1510, 1998.

893 Berg, P., Rysgaard, S., and Thamdrup, B.: Dynamic modeling of early diagenesis and nutrient  
894 cycling. A case study in an Arctic marine sediment, *Amer. J. Sci*, 303, 906-955, 2003.

895 Boetius, A., and Damm, E.: Benthic oxygen uptake, hydrolytic potentials and microbial  
896 biomass at the Arctic continental slope, *Deep Sea Research Part I: Oceanographic Research*  
897 *Papers*, 45, 239-275, 1998.

898 Boudreau, B. P.: *Diagenetic models and their implementation*, Springer Verlag, 414 pp.,  
899 1996.

900 Bourgeois, S., Archambault, P., and Witte, U.: Organic matter remineralization in marine  
 901 sediments: A Pan-Arctic synthesis, *Global Biogeochemical Cycles*, 31, 190-213, 2017.

902 Bröder, L.-M., Tesi, T., Salvado, J. A., Semiletov, I., Dudarev, O. V., and Gustafsson, Ö.:  
 903 Fate of terrigenous organic matter across the Laptev Sea from the mouth of the Lena River to  
 904 the deep sea of the Arctic interior, *Biogeosciences*, 13, 5003-5019, 2016a.

905 Bröder, L., Tesi, T., Andersson, A., Eglinton, T. I., Semiletov, I. P., Dudarev, O. V., Roos, P.,  
 906 and Gustafsson, Ö.: Historical records of organic matter supply and degradation status in the  
 907 East Siberian Sea, *Organic Geochemistry*, 91, 16-30, 2016b.

908 Canfield, D. E., Kristensen, E., and Thamdrup, B.: Aquatic geomicrobiology, *Advances in*  
 909 *marine biology*, 48, 2005.

910 Dmitrenko, I. A., Tyshko, K. N., Kirillov, S. A., Eicken, H., Hölemann, J. A., and Kassens,  
 911 H.: Impact of flaw polynyas on the hydrography of the Laptev Sea, *Global and Planetary*  
 912 *Change*, 48, 9-27, 2005.

913 Dmitrenko, I. A., Kirillov, S. A., and Tremblay, L. B.: The long-term and interannual  
 914 variability of summer fresh water storage over the eastern Siberian shelf: Implication for  
 915 climatic change, *Journal of Geophysical Research: Oceans*, 113, doi: 10.1029/2007JC004304,  
 916 2008.

917 Dudarev, O. V., Semiletov, I. P., and Charkin, A. N.: Particulate material composition in the  
 918 Lena River-Laptev Sea system: Scales of heterogeneities. In: *Doklady Earth Sciences*, 6,  
 919 1000-1005, 2006.

920 Fahl, K., and Nöthig, E.-M.: Lithogenic and biogenic particle fluxes on the Lomonosov Ridge  
 921 (central Arctic Ocean) and their relevance for sediment accumulation: Vertical vs. lateral  
 922 transport, *Deep Sea Research Part I: Oceanographic Research Papers*, 54, 1256-1272, 2007.

923 Glud, R. N.: Oxygen dynamics of marine sediments, *Mar. Biol. Res.*, 4, 243-289, 2008.

924 Grebmeier, J. M., Cooper, L. W., Feder, H. M., and Sirenko, B. I.: Ecosystem dynamics of the  
 925 Pacific-influenced Northern Bering and Chukchi Seas in the Amerasian Arctic, *Progress in*  
 926 *Oceanography*, 71, 331-361, 2006.

927 Guay, C. K., Falkner, K. K., Muench, R. D., Mensch, M., Frank, M., and Bayer, R.: Wind-  
 928 driven transport pathways for Eurasian Arctic river discharge, *Journal of Geophysical*  
 929 *Research: Oceans*, 106, 11469-11480, 2001.

930 Guo, L., Ping, C. L., and Macdonald, R. W.: Mobilization pathways of organic carbon from  
 931 permafrost to arctic rivers in a changing climate, *Geophysical Research Letters*, 34, 2007.

932 Hall, P. O. J., and Aller, R. C.: Rapid, small-volume flow injection analysis for  $\Sigma\text{CO}_2$  and  
 933  $\text{NH}_4^+$  in marine and freshwaters, *Limnology and Oceanography*, 37, 1113-1119, 1992.

934 Hugelius, G., Strauss, J., Zubrzycki, S., Harden, J. W., Schuur, E. A. G., Ping, C. L.,  
 935 Schirmer, L., Grosse, G., Michaelson, G. J., Koven, C. D., O'Donnell, J. A., Elberling, B.,  
 936 Mishra, U., Camill, P., Yu, Z., Palmtag, J., and Kuhry, P.: Estimated stocks of circumpolar  
 937 permafrost carbon with quantified uncertainty ranges and identified data gaps,  
 938 *Biogeosciences*, 11, 6573-6593, 2014.

939 Ivanov, V. V. and Golovin, P. N.: Observations and modeling of dense water cascading from  
 940 the northwestern Laptev Sea shelf, *Journal of Geophysical Research: Oceans*, 112, 2007.

941 Jørgensen, B. B.: A comparison of methods for the quantification of bacterial sulfate  
 942 reduction in coastal marine sediments: I. Measurement with radiotracer techniques,  
 943 *Geomicrobiology Journal*, 1, 11-27, 1978.

944 Jørgensen, B. B., and Kasten, S.: Sulfur and methane oxidation, in: *Marine Geochemistry*,  
 945 Second Edition ed., edited by: Schulz, H. D., and Zabel, M., Springer Verlag, Berlin  
 946 Heidelberg, 271-309, 2006.

947 Kallmeyer, J., Ferdelman, T. G., Weber, A., Fossing, H., and Jørgensen, B. B.: Evaluation of  
 948 a cold chromium distillation procedure for recovering very small amounts of radiolabeled  
 949 sulfide related to sulfate reduction measurements., *Limnol. Oceanog. Methods*, 2, 171-180,  
 950 2004.

951 Karlsson, E. S., Brüchert, V., Tesi, T., Charkin, A., Dudarev, O., Semiletov, I., and  
 952 Gustafsson, Ö.: Contrasting regimes for organic matter degradation in the East Siberian Sea  
 953 and the Laptev Sea assessed through microbial incubations and molecular markers, *Marine*  
 954 *Chemistry*, 170, 11-22, 2015.

955 Koven, C. D., Lawrence, D. M., and Riley, W. J.: Permafrost carbon-climate feedback is  
 956 sensitive to deep soil carbon decomposability but not deep soil nitrogen dynamics,  
 957 *Proceedings of the National Academies of Science*, 112, 3752-3757, 2015.

958 Lalonde, K., Mucci, A., Ouellet, A., and Gelinas, Y.: Preservation of organic matter in  
 959 sediments promoted by iron, *Nature*, 483, 198-200, 2012.

960 Li, Y.-H. and Gregory, S.: Diffusion of ions in sea water and in deep-sea sediments,  
 961 *Geochimica et Cosmochimica Acta*, 88, 703-714, 1974.

962 Macdonald, R. W., and Gobeil, C.: Manganese Sources and Sinks in the Arctic Ocean with  
 963 Reference to Periodic Enrichments in Basin Sediments, *Aquatic Geochemistry*, 18, 565-591,  
 964 2012.

965 Mackin, J. E., and Aller, R.C.: Ammonium adsorption in marine sediments, *Limnology and*  
 966 *Oceanography*, 29, 250-257, 1984.

967 Macdonald, R. W., Kuzyk, Z. Z. A., and Johannessen, S. C.: The vulnerability of Arctic shelf  
 968 sediments to climate change, *Environmental Reviews*, 1-19, 2015.

969 McGuire, A. D., Anderson, L. G., Christensen, T. R., Dallimore, S., Guo, L., Hayes, D. J.,  
 970 Heimann, M., Lorenson, T. D., Macdonald, R. W., and Roulet, N.: Sensitivity of the carbon  
 971 cycle in the Arctic to climate change, *Ecological Monographs*, 79, 523-555, 2009.

972 McTigue, N., Gardner, W., Dunton, K., and Hardison, A.: Biotic and abiotic controls on co-  
 973 occurring nitrogen cycling processes in shallow Arctic shelf sediments, *Nature*  
 974 *Communications*, 7, 2016.

975 Miller, C. M., Dickens, G. R., Jakobsson, M., Johansson, C., Koshurnikov, A., O'Regan, M.,  
 976 Muschitiello, F., Stranne, C., and Mörtz, C.-M.: Low methane concentrations in sediment  
 977 along the continental slope north of Siberia: Inference from pore water geochemistry,  
 978 *Biogeosciences Discussions*, doi:10.5194/bg-2016-308, 2016.

979 Naidu, A. S., Cooper, L. W., Finney, B. P., Macdonald, R. W., Alexander, C., and Semiletov,  
 980 I. P.: Organic carbon isotope ratios ( $\delta^{13}\text{C}$ ) of Arctic Amerasian Continental shelf sediments.  
 981 *International Journal of Earth Sciences*, 89, 522-532, 2000.

982 Nickel, M., Vandieken, V., Brüchert, V., and Jørgensen, B. B.: Microbial Mn(IV) and Fe(III)  
 983 reduction in northern Barents Sea sediments under different conditions of ice cover and

984 organic carbon deposition, *Deep Sea Research Part II: Topical Studies in Oceanography*, 55,  
985 2390-2398, 2008.

986 Nitishinsky, M., Anderson, L. G., and Hölemann, J. A.: Inorganic carbon and nutrient fluxes  
987 on the Arctic Shelf, *Continental Shelf Research*, 27, 1584-1599, 2007.

988 Pipko, I., Semiletov I.P., Pugach S.P., Wahlstrom I., Anderson L.G. Interannual variability of  
989 air-sea CO<sub>2</sub> fluxes and carbon system in the East Siberian Sea. *Biogeosciences*, 8, 1987-2007,  
990 2011.

991 Pivovarov, S., Hölemann, J., Kassens, H., Antonow, M., and Dmitrenko, I.: Dissolved  
992 oxygen, silicon, phosphorous and suspended matter concentrations during the spring breakup  
993 of the Lena River, in: *Land–Ocean Systems in the Siberian Arctic: Dynamics and History*,  
994 edited by: Kassens, H., Bauch, H. A., Dmitrenko, I., Eicken, H., Hubberten, H.-W., Melles,  
995 M., Thiede, J., and Timokhov, L., Springer, Berlin, 251-264, 1999.

996 Qi, D., Chen, L., Chen, B., Gao, Z., Zhong, W., Feely, R. A., Anderson, L. G., Sun, H., Chen,  
997 J., Chen, M., Zhan, L., Zhang, Y., and Cai, W.-J.: Increase in acidifying water in the western  
998 Arctic Ocean, *Nature Clim. Change*, 7, 195-199, 2017.

999 Rachold, V., Eicken, H., Gordeev, V., Grigoriev, M. N., Hubberten, H.-W., Lisitzin, A. P.,  
1000 Shevchenko, V., and Schirrmeister, L.: Modern terrigenous organic carbon input to the Arctic  
1001 Ocean, in: *The organic carbon cycle in the Arctic Ocean*, Springer, 33-55, 2004.

1002 Rasmussen, H., and Jørgensen, B. B.: Microelectrode studies of seasonal oxygen uptake in a  
1003 coastal sediment: Role of molecular diffusion, *Marine ecology progress series*. Oldendorf, 81,  
1004 289-303, 1992.

1005 Raymond, P. A., McClelland, J., Holmes, R., Zhulidov, A., Mull, K., Peterson, B., Striegl, R.,  
1006 Aiken, G., and Gurtovaya, T.: Flux and age of dissolved organic carbon exported to the Arctic  
1007 Ocean: A carbon isotopic study of the five largest arctic rivers, *Global Biogeochemical*  
1008 *Cycles*, 21, 10.1029/2007GB002983, 2007.

1009 Rekant, P., Bauch, H. A., Schwenk, T., Portnov, A., Gusev, E., Spiess, V., Cherkashov, G.,  
1010 and Kassens, H.: Evolution of subsea permafrost landscapes in Arctic Siberia since the Late  
1011 Pleistocene: a synoptic insight from acoustic data of the Laptev Sea, *Arktos*, 1,  
1012 10.1007/s41063-015-0011-y, 2015.

1013 Rossel, P. E., Bienhold, C., Boetius, A., and Dittmar, T.: Dissolved organic matter in pore  
 1014 water of Arctic Ocean sediments: Environmental influence on molecular composition,  
 1015 *Organic Geochemistry*, 97, 41-52, 2016.

1016 Sakshaug, E.: Primary and secondary production in the Arctic Seas, in: *The organic carbon*  
 1017 *cycle in the Arctic Ocean*, Springer, 57-81, 2004.

1018 Salvadó, J. A., Tesi, T., Andersson, A., Ingri, J., Dudarev, O. V., Semiletov, I. P., and  
 1019 Gustafsson, Ö.: Organic carbon remobilized from thawing permafrost is resequenced by  
 1020 reactive iron on the Eurasian Arctic Shelf, *Geophysical Research Letters*, 42, 8122-8130,  
 1021 2015.

1022 Sánchez-García, L., Alling, V., Pugach, S., Vonk, J., van Dongen, B., Humborg, C., Dudarev,  
 1023 O., Semiletov, I., and Gustafsson, Ö.: Inventories and behavior of particulate organic carbon  
 1024 in the Laptev and East Siberian seas, *Global Biogeochemical Cycles*, 25,  
 1025 10.1029/2010gb003862, 2011.

1026 Savvichev, A., Rusanov, I., Pimenov, N., Zakharova, E., Veslopolova, E., Lein, A. Y., Crane,  
 1027 K., and Ivanov, M.: Microbial processes of the carbon and sulfur cycles in the Chukchi Sea,  
 1028 *Microbiology*, 76, 603-613, 2007.

1029 Schuur, E. A. G., McGuire, A. D., Schadel, C., Grosse, G., Harden, J. W., Hayes, D. J.,  
 1030 Hugelius, G., Koven, C. D., Kuhry, P., Lawrence, D. M., Natali, S. M., Olefeldt, D.,  
 1031 Romanovsky, V. E., Schaefer, K., Turetsky, M. R., Treat, C. C., and Vonk, J. E.: Climate  
 1032 change and the permafrost carbon feedback, *Nature*, 520, 171-179, 2015.

1033 Seeberg-Elverfeldt, J., Schlüter, M., Feseker, T., and Kölling, M.: Rhizon sampling of  
 1034 porewaters near the sediment-water interface of aquatic systems, *Limnol. Oceanogr. Methods*,  
 1035 3, 361-371, 2005.

1036 Semiletov, I., Dudarev, O., Luchin, V., Charkin, A., Shin, K.-H., and Tanaka, N.: The East  
 1037 Siberian Sea as a transition zone between Pacific-derived waters and Arctic shelf waters,  
 1038 *Geophysical Research Letters*, 10.1029/2005GL022490, 2005.

1039 Semiletov, I., Pipko, I., Gustafsson, Ö., Anderson, L. G., Sergienko, V., Pugach, S., Dudarev,  
 1040 O., Charkin, A., Gukov, A., Broder, L., Andersson, A., Spivak, E., and Shakhova, N.:  
 1041 Acidification of East Siberian Arctic Shelf waters through addition of freshwater and  
 1042 terrestrial carbon, *Nature Geoscience*, 9, 361-365, 2016.



1043 Semiletov I.P., Shakhova, N.E, Pipko, I.I.: Space-time dynamics of carbon and environmental  
 1044 parameters related to carbon dioxide emissions in the Buor-Khaya Bay and adjacent part of  
 1045 the Laptev Sea. *Biogeosciences*, **10**, 5977-5996, 2013.

1046 Semiletov I.P., Pipko I.I., Shakhova N.E., Dudarev O.V., Pugach S.P., Charkin A.N., McRoy  
 1047 C.P., Kosmach D., and Ö. Gustafsson.: Carbon transport by the Lena River from its  
 1048 headwaters to the Arctic Ocean, with emphasis on fluvial input of terrestrial particulate  
 1049 organic carbon vs. carbon transport by coastal erosion. *Biogeosciences*, **8**, 2407-2426, 2011.

1050 Semiletov, I.P., Destruction of the coastal permafrost ground as an important factor in  
 1051 biogeochemistry of the Arctic Shelf waters, *Trans. (Doklady) Russian Acad. Sci.*, 368, 679-  
 1052 682, 1999 (translated into English).

1053 Stein, R., and Macdonald, R. W.: *The Organic Carbon Cycle in the Arctic Ocean*, Springer-  
 1054 Verlag, Berlin, 382 pp., 2004.

1055 Strobl, C., Schulz, V., Vogler, S., Baumann, S., Kassens, H., Kubik, P. W., Suter, M., and  
 1056 Mangini, A.: Determination of depositional beryllium-10 fluxes in the area of the Laptev Sea  
 1057 and beryllium-10 concentrations in water samples of high northern latitudes, in: *Land-Ocean*  
 1058 *Systems in the Siberian Arctic: Dynamics and History*, edited by: Kassens, H., Bauch, H. A.,  
 1059 Dmitrenko, I., Eicken, H., Hubberten, H.-W., Melles, M., Thiede, J., and Timokhov, L.,  
 1060 Springer, Berlin, 515-532, 1998.

1061 Tarnocai, C., Canadell, J. G., Schuur, E. A. G., Kuhry, P., Mazhitova, G., and Zimov, S.: Soil  
 1062 organic carbon pools in the northern circumpolar permafrost region, *Global Biogeochemical*  
 1063 *Cycles*, **23**, 10.1029/2008gb003327, 2009.

1064 Tesi, T., Semiletov, I., Hugelius, G., Dudarev, O., Kuhry, P., and Gustafsson, Ö.:  
 1065 Composition and fate of terrigenous organic matter along the Arctic land–ocean continuum in  
 1066 East Siberia: Insights from biomarkers and carbon isotopes, *Geochimica et Cosmochimica*  
 1067 *Acta*, **133**, 235-256, 2014.

1068 Tesi, T., Semiletov, I., Dudarev, O., Andersson, A., and Gustafsson, Ö.: Matrix association  
 1069 effects on hydrodynamic sorting and degradation of terrestrial organic matter during cross-  
 1070 shelf transport in the Laptev and East Siberian shelf seas, *Journal of Geophysical Research:*  
 1071 *Biogeosciences*, **121**, 731-752, 2016.

1072 [Tesi, T., Geibel, M. C., Pearce, C., Panova, E., Vonk, J. E., Karlsson, E., Salvado, J. A.,](#)  
1073 [Kruså, M., Bröder, L., Humborg, C., Semiletov, I., and Gustafsson, Ö.: Carbon geochemistry](#)  
1074 [of plankton-dominated samples in the Laptev and East Siberian shelves: contrasts in](#)  
1075 [suspended particle composition, \*Ocean Sci.\*, 13, 735-748, 10.5194/os-13-735-2017, 2017.](#)

1076 Thamdrup, B.: Bacterial manganese and iron reduction in aquatic sediments, *Advances in*  
1077 *Microbial Ecology*, 16, 41-84, 2000.

1078 Arrigo, K. R., and van Dijken, G. L.: Secular trends in Arctic Ocean net primary production,  
1079 *Journal of Geophysical Research: Oceans*, 116, 10.1029/2011JC007151, 2011.

1080 Hugelius, G., Strauss, J., Zubrzycki, S., Harden, J. W., Schuur, E. A. G., Ping, C. L.,  
1081 Schirrmeister, L., Grosse, G., Michaelson, G. J., Koven, C. D., O'Donnell, J. A., Elberling, B.,  
1082 Mishra, U., Camill, P., Yu, Z., Palmtag, J., and Kuhry, P.: Estimated stocks of circumpolar  
1083 permafrost carbon with quantified uncertainty ranges and identified data gaps,  
1084 *Biogeosciences*, 11, 6573-6593, 2014.

1085 Qi, D., Chen, L., Chen, B., Gao, Z., Zhong, W., Feely, R. A., Anderson, L. G., Sun, H., Chen,  
1086 J., Chen, M., Zhan, L., Zhang, Y., and Cai, W.-J.: Increase in acidifying water in the western  
1087 Arctic Ocean, *Nature Clim. Change*, 7, 195-199, 2017.

1088 Sánchez-García, L., Alling, V., Pugach, S., Vonk, J., van Dongen, B., Humborg, C., Dudarev,  
1089 O., Semiletov, I., and Gustafsson, Ö.: Inventories and behavior of particulate organic carbon  
1090 in the Laptev and East Siberian seas, *Global Biogeochemical Cycles*, 25,  
1091 10.1029/2010gb003862, 2011.

1092 Vandieken, V., Nickel, M., and Jørgensen, B. B.: Carbon mineralization in Arctic sediments  
1093 northeast of Svalbard: (Mn(IV) and Fe(III) reduction as principal anaerobic respiratory  
1094 pathways, *Marine Ecology Progress Series*, 322, 15-27, 2006.

1095 Vonk, J. E., Sanchez-Garcia, L., van Dongen, B. E., Alling, V., Kosmach, D., Charkin, A.,  
1096 Semiletov, I. P., Dudarev, O. V., Shakhova, N., Roos, P., Eglinton, T. I., Andersson, A., and  
1097 Gustafsson, O.: Activation of old carbon by erosion of coastal and subsea permafrost in Arctic  
1098 Siberia, *Nature*, 489, 137-140.

1099 Wegner, C., Hölemann, J. A., Dmitrenko, I., Kirillov, S., and Kassens, H.: Seasonal variations  
1100 in Arctic sediment dynamics—evidence from 1-year records in the Laptev Sea (Siberian  
1101 Arctic), *Global and Planetary Change*, 48, 126-140, 2005.

1102 Wegner, C., Bauch, D., Hölemann, J. A., Janout, M. A., Heim, B., Novikhin, A., Kassens, H.,  
1103 and Timokhov, L.: Interannual variability of surface and bottom sediment transport on the  
1104 Laptev Sea shelf during summer, *Biogeosciences*, 10, 1117-1129, 2013.

1105 Weingartner, T. J., Danielson, S., Sasaki, Y., Pavlov, V., and Kulakov, M.: The Siberian  
1106 Coastal Current: A wind- and buoyancy-forced Arctic coastal current, *Journal of Geophysical*  
1107 *Research: Oceans*, 104, 29697-29713, 1999.

1108

1109

1110

Table 1. Physical and chemical characteristics of sediment and bottom water at the sampled stations

Station	Latitude °N	Longitude °E	Date	Water depth m	Ice cover %	Bottom water salinity ‰	Bottom water temperature °C	Bottom water O <sub>2</sub> concentration μmol/L	Bottom water NH <sub>4</sub> <sup>+</sup> concentration μmol/L	Bottom water DIC above sediment μmol/L	δ <sup>13</sup> C DIC bottom water ‰ vs. VPDB	Sediment description
1	78.942	125.243	7/15/2014	3146	50 - 75	34.9	-0.9	271.9	1.65	2151.5	-0.5	clay, brown
2	78.581	125.607	7/16/2014	2900	25 - 50	34.9	-0.9	275.0	n.a.	n.a.	n.a.	clay, brown
3	78.238	126.150	7/16/2014	2601	<25	34.9	-0.9	280.0	n.a.	n.a.	n.a.	clay, brown
4	77.855	126.664	7/16/2014	2106	<25	34.9	-0.8	289.4	1.81	2164.5	-1.6	clay, brown
6	77.142	127.378	7/17/2014	89	0.0	34.6	-1.8	327.0	1.30	2213.0	-2.2	clay, top 3 cm brown, then gray, fauna on top of sediment
23	76.171	129.333	7/22/2014	56	0.0	34.2	-1.8	303.2	1.34	2246.3	-3.2	silty clay, top 4 cm brown, then gray, brittle stars
24	75.599	129.558	7/24/2014	46	0.0	34.0	-1.7	283.8	0.89	2244.1	-2.0	silty clay, top 4 cm brown, then gray
27	76.943	132.229	7/25/2014	44	0.0	34.2	-1.8	332.3	0.94	2295.0	-6.5	silty clay, top 2 cm brown, then gray, fluffy surface layer, brittle stars
30	78.181	138.354	7/24/2014	69	0.0	34.1	-1.6	334.8	0.79	2178.4	-3.7	silty clay, top 4 cm brown, then gray
31	79.396	135.497	7/25/2014	3056	0.0	34.9	-0.9	270.9	0.74	2161.7	n.a.	clay, brown
35	78.600	137.061	7/26/2014	541	0.0	34.9	0.4	288.1	0.43	2183.7	n.a.	clay top 15 cm brown, fluffy, inhomogeneous, surface- dwelling fauna
37	78.521	137.170	7/26/2014	205	0.0	34.7	0.0	295.4	0.89	2171.1	n.a.	clay, top 5 cm brown, then gray
40	77.670	144.668	7/27/2014	45	0.0	31.5	-1.3	190.3	0.53	2213.7	-1.6	silty clay, top 3 cm brown, then gray, brittle stars
43	76.780	147.791	7/28/2014	42	25-50	30.1	-1.2	256.4	0.61	2086.7	n.a.	silty clay to clayey silt, top 2 cm brown, then gray, some small surface-dwelling animals
45	76.416	148.115	7/29/2014	40	<50	29.1	-1.3	319.9	0.57	22576.0	-2.1	silty clay to clayey silt, 2 cm brown, then gray-black, rather stiff
48	76.615	153.345	7/30/2014	49	>75	30.6	-1.6	315.9	0.50	2075.1	-2.2	silty clay to clayey silt, top 3 cm brown, then gray/black
50	75.764	158.529	8/1/2014	44	>75	31.1	-1.4	311.0	0.51	2068.7	-2.1	silty clay to clayey silt, top 2 cm brown, then gray/black
53	74.957	161.088	8/2/2014	47	>75	31.0	-1.6	253.3	0.16	2086.1	-2.5	silty clay to clayey silt, top 3 cm brown, then 3 cm gray, then gray/black
58	74.440	166.050	8/4/2014	54	>75	31.4	-1.7	254.3	0.65	2154.9	-1.5	silty clay to clayey silt, slightly resuspended, top 2 cm brown, then gray, soft
63	74.685	172.361	8/7/2014	67	>75	32.4	-1.4	186.0	0.61	2240.8	-2.2	silty clay to clayey silt, top 1 cm brown, then gray

Formatted: English (United States)

1113

Table 2. O<sub>2</sub> uptake, integrated <sup>35</sup>S-sulfate reduction rates, DIC flux, and porewater DIC/NH<sub>4</sub><sup>+</sup> ratios

Station	Water depth	mean O <sub>2</sub> penetration depth	mean O <sub>2</sub> at 60mm depth	O <sub>2</sub> uptake (modelled/measured with 2D optode)	<sup>35</sup> S-SRR (0-30 cm) duplicates	DIC flux (modelled in anaerobic zone/measured with whole core incubation)	Average porewater DIC/NH <sub>4</sub> <sup>+</sup>
	m	mm	μmol/L	mmol m <sup>-2</sup> d <sup>-1</sup>	mmol m <sup>-2</sup> d <sup>-1</sup>	mmol m <sup>-2</sup> d <sup>-1</sup>	
1	3146	> 60	217	1.48 ± 0.08	0.05 / 0.21	-0.11	
2	2900	> 60	213	1.32 ± 0.05			
3	2601	> 60	194	0.81 ± 0.06			
4	2106	> 60	89	1.32 ± 0.05	0.17 / 0.17	-0.15	
6	89	36	0	2.61 ± 0.01	0.03 / 0.05	-0.08	
23	56	13	0	5.00 ± 0.09 ; 5.3 ± 0.2	0.56	-0.12; -5.1 ± 0.4	13
24	46	10	0	7.95 ± 0.14		-0.22	10
27	44	16	0	3.75 ± 0.08	0.37 / 0.20	-0.27	12
30	69	16	0	2.61 ± 0.11	0.06 / 0.03	-0.12	15
31	3056	> 60	194	1.78 ± 0.07			
35	541	> 60	30	2.43 ± 0.32			
37	205	44	0	2.51 ± 0.10			
Average Laptev Sea shelf				4.20	0.19	0.2 ; 5.1	12
40	45	12	0	4.62 ± 0.08	0.33 / 0.24	-0.19	16
43	42	13	0	4.7 ± 0.10			
45	40	10	0	4.02 ± 0.10	0.23 / 0.19	-0.37	13
48	49	5	0	9.14 ± 0.22	0.68 / 0.53	-0.71	10
50	44	9	0	5.65 ± 0.43; 5.2 ± 0.1	1.32 / 1.40	-1.01 ; -5.2 ± 0.2	12
53	47	10	0	4.53 ± 0.08 ; 4.7 ± 0.1	0.10 / 0.17	-0.20	14
58	54	3	0	11.49 ± 0.52	1.01	-1.27	24
63	67	4	0	0.72 ± 0.15 ; 10.8 ± 0.1	1.41	-1.35 ; -10.8 ± 0.6	12
Average East Siberian Sea shelf				7.2		0.7 ; 8.0	14

1114

1115

Formatted: English (United States)

Formatted: Font: Not Bold

1116	<u>List of Tables</u>
1117	
1118	<u>Table 1. Physical and chemical characteristics of sediment and bottom water chemical</u>
1119	<u>characteristics at the sampled stations.</u>
1120	<u>Table 2. O<sub>2</sub> uptake, integrated <sup>35</sup>S-sulfate reduction rates, DIC flux, and porewater DIC/NH<sub>4</sub><sup>±</sup></u>
1121	<u>ratios.</u>
1122	<u>Table 3. Anaerobic rates of carbon mineralization by manganese, iron, and sulfate reduction.</u>
1123	<u>Table 4. Calculated carbon isotope composition of remineralized DIC and mass fractions of</u>
1124	<u>the marine and terrestrial end member and corresponding terrestrial carbon degradation rates</u>
1125	<u>based on <sup>35</sup>S-SRR and DIC.</u>
1126	<u>Table 5. Regional estimates of sediment carbon mineralization in the outer Laptev and East</u>
1127	<u>Siberian shelf sea.</u>

## List of figures

Fig. 1: General map of the Laptev and East Siberian Sea with sediment stations and major current features

Fig. 2: Depth profiles of dissolved O<sub>2</sub> measured with O<sub>2</sub> microelectrode sensors for Stations 1, 23, 30, 45, 58, and 63 and profiles of porewater concentrations of dissolved iron and manganese.

Fig. 3: <sup>35</sup>S-SRR rates and corresponding porewater sulfate concentrations for Stations 1, 23, 30, 45, 58, and 63.

Fig 4: Depth profiles of dissolved inorganic carbon (DIC),  $\delta^{13}\text{C}_{\text{DIC}}$ , and dissolved ammonium (NH<sub>4</sub><sup>+</sup>) for Stations 1, 23, 30, 45, 58, and 63.

Fig. 5 A: Crossplot of dissolved NH<sub>4</sub><sup>+</sup> and porewater DIC\* after correction for bottom water DIC concentrations. The average porewater DIC/NH<sub>4</sub><sup>+</sup> ratios for the individual stations are shown in Table 2. B: Keeling plot of the fraction of remineralized DIC calculated from a two endmember mixing model versus  $\delta^{13}\text{C}_{\text{DIC}}$ .

Fig. 6. Comparison of reaction rates of oxygen, manganese, iron, and sulfate reduction at Station 23. Note the different depth scale for the O<sub>2</sub> consumption rate. The dashed line marks the oxygen penetration depth.

Fig. 7. Crossplot of diffusive oxygen uptake and integrated sulfate reduction rates. The black line is the result of the regression analysis that yielded a y-intercept of 2.1 mmol m<sup>-2</sup> d<sup>-1</sup> and a slope of 6.1 ± 0.1. Blue and red lines show the 95% and 99% confidence interval.

Formatted: Font: Times New Roman, 12 pt

1154 Fig. 8 A. Map of field area and sampling stations showing oxygen uptake rates. For  
1155 comparison, oxygen uptake rates reported in Boetius and Damm (1998) are shown as triangles  
1156 using the same color code. B: Map of field area and sampling stations with depth-integrated  
1157 sulfate reduction rates.

Formatted: Font: Times New Roman, 12 pt

1158 ▲  
1159 Fig. 9 A. Water depth variation of sediment oxygen uptake. B: Water depth variation of  
1160 integrated <sup>35</sup>S-sulfate reduction rates (0-30 cm sediment depth). For reference average rates of  
1161 abyssal plain, continental rise, slope, and shelf sediments, deposition and non-depositional,  
1162 are shown for reference.

Formatted: Font: Times New Roman, 12 pt, English (United States)

Formatted: Line spacing: 1.5 lines

Formatted: Font: Times New Roman, 12 pt



Table 1. Physical and chemical characteristics of sediment and bottom water at the sampled stations

Station	Latitude °N	Longitude °E	Date	Water depth m	Ice cover %	Bottom water salinity	Bottom water temperature °C	Bottom water O <sub>2</sub> µmol/L	Bottom water NH <sub>4</sub> <sup>+</sup> concentration µmol/L	Bottom water DIC above sediment µmol/L	% vs. VPDB	δ <sup>13</sup> C DIC bottom water ‰	δ <sup>13</sup> C surface sediment ‰	Sediment description
1	76.942	125.543	Month/Day/Year	m	%	‰	°C	µmol/L	µmol/L	µmol/L	% vs. VPDB	‰	‰	
1	76.942	125.543	7/15/2014	3146	50-75	34.9	-0.9	271.9	1.65	2151.5	-0.5	-22.3		clay, brown
2	78.581	125.607	7/16/2014	2900	25-50	34.9	-0.9	275.0	n.a.	n.a.	n.a.	n.a.	n.a.	clay, brown
3	78.238	126.150	7/16/2014	2601	<25	34.9	-0.9	280.0	n.a.	n.a.	n.a.	n.a.	n.a.	clay, brown
4	77.855	126.664	7/16/2014	2106	<25	34.9	-0.8	289.4	1.81	2164.5	-1.6	-22.5		clay, brown
6	77.142	127.378	7/17/2014	89	0.0	34.6	-1.8	327.0	1.30	2213.0	-2.2	-23.2		clay, top 3 cm brown, then gray, flume on top of sediment
23	76.171	129.333	7/22/2014	56	0.0	34.2	-1.8	303.2	1.34	2246.3	-3.2	-25.0		silty clay, top 4 cm brown, then gray, brittle stars
24	75.599	129.558	7/24/2014	46	0.0	34.0	-1.7	283.8	0.89	2244.1	-2.0	-24.8		silty clay, top 4 cm brown, then gray
27	76.943	132.229	7/23/2014	44	0.0	34.2	-1.8	332.3	0.94	2595.0	-6.5	-24.2		silty clay, top 2 cm brown, then gray, fluffy surface layer, brittle stars
30	78.181	138.354	7/24/2014	69	0.0	34.1	-1.6	334.8	0.79	2178.4	-3.7	-23.4		silty clay, top 4 cm brown, then gray
31	79.396	135.497	7/25/2014	3056	0.0	34.9	-0.9	270.9	0.74	2161.7	n.a.	n.a.		clay, brown
35	78.600	137.061	7/26/2014	541	0.0	34.9	0.4	288.1	0.45	2183.7	n.a.	n.a.		clay top 15cm brown, fluffy, homogeneous, surface-cracking flume
37	78.521	137.170	7/26/2014	205	0.0	34.7	0.0	295.4	0.89	2171.1	n.a.	n.a.		clay, top 5cm brown, then gray
40	77.670	144.668	7/27/2014	45	0.0	31.5	-1.3	190.3	0.53	2213.7	-1.6	-23.7		silty clay top 3cm brown, then gray, brittle stars
43	76.780	147.791	7/28/2014	42	25-50	30.1	-1.2	256.4	0.61	2086.7	n.a.	n.a.		silty clay to clayey silt, top 2cm brown, then gray, some small surface-dwelling animals
45	76.416	148.115	7/29/2014	40	< 50	29.1	-1.3	319.9	0.57	2576.0	-2.1	-24.4		silty clay to clayey silt, 2cm brown, then gray-black, rather stiff
48	76.615	153.345	7/30/2014	49	> 75	30.6	-1.6	315.9	0.50	2075.1	-2.2	-25.8		silty clay to clayey silt, top 3cm brown, then gray/black
50	75.764	158.529	8/1/2014	44	> 75	31.1	-1.4	311.0	0.51	2068.7	-2.1	-24.6		silty clay to clayey silt, top 2cm brown, then gray/black
53	74.957	161.088	8/2/2014	47	> 75	31.0	-1.6	253.3	0.16	2086.1	-2.5	n.a.		silty clay to clayey silt, top 3 cm brown, then 3 cm gray, then gray/black
58	74.440	166.050	8/4/2014	54	> 75	31.4	-1.7	254.3	0.65	2154.9	-1.5	-23.8		silty clay to clayey silt, slightly resuspended, top 2 cm brown, then gray/black
63	74.685	172.561	8/7/2014	67	> 75	32.4	-1.4	186.0	0.61	2240.8	-2.2	-22.7		silty clay to clayey silt, top 1cm brown, then gray

1168

Table 2. O<sub>2</sub> uptake, integrated <sup>35</sup>S-sulfate reduction rates, DIC flux, and porewater DIC/NH<sub>4</sub><sup>+</sup> ratios

Station	Water depth	mean O <sub>2</sub> penetration depth	mean O <sub>2</sub> at 60mm depth	O <sub>2</sub> uptake (modelled/measured with 2D optode)	<sup>35</sup> S-SRR (0-30 cm) duplicates	DIC flux (modelled in anaerobic zone/measured with whole core incubation)	Average porewater DIC/NH <sub>4</sub> <sup>+</sup>
	m	mm	μmol/L	mmol m <sup>-2</sup> d <sup>-1</sup>	mmol m <sup>-2</sup> d <sup>-1</sup>	mmol m <sup>-2</sup> d <sup>-1</sup>	
1	3146	> 60	217	1.48 ± 0.08	0.05 / 0.21	-0.11	
2	2900	> 60	213	1.32 ± 0.05			
3	2601	> 60	194	0.81 ± 0.06			
4	2106	> 60	89	1.32 ± 0.05	0.17 / 0.17	-0.15	
6	89	36	0	2.61 ± 0.01	0.03 / 0.05	-0.08	
23	56	13	0	5.00 ± 0.09 ; 5.3 ± 0.2	0.56	-0.12; -5.1 ± 0.4	13
24	46	10	0	7.95 ± 0.14		-0.22	10
27	44	16	0	3.75 ± 0.08	0.37 / 0.20	-0.27	12
30	69	16	0	2.61 ± 0.11	0.06 / 0.03	-0.12	15
31	3056	> 60	194	1.78 ± 0.07			
35	541	> 60	30	2.43 ± 0.32			
37	205	44	0	2.51 ± 0.10			
Average Laptev Sea shelf				4.20	0.19	0.2 ; 5.1	12
40	45	12	0	4.62 ± 0.08	0.33 / 0.24	-0.19	16
43	42	13	0	4.7 ± 0.10			
45	40	10	0	4.02 ± 0.10	0.23 / 0.19	-0.37	13
48	49	5	0	9.14 ± 0.22	0.68 / 0.53	-0.71	10
50	44	9	0	5.65 ± 0.43; 5.2 ± 0.1	1.32 / 1.40	-1.01 ; -5.2 ± 0.2	12
53	47	10	0	4.53 ± 0.08 ; 4.7 ± 0.1	0.10 / 0.17	-0.20	14
58	54	3	0	11.49 ± 0.52	1.01	-1.27	24
63	67	4	0	10.72 ± 0.15 ; 10.8 ± 0.3	1.41	-1.35 ; -10.8 ± 0.6	12
Average East Siberian Sea shelf				7.2		0.7 ; 8.0	14

1169

1170

1171

Formatted: English (United States)

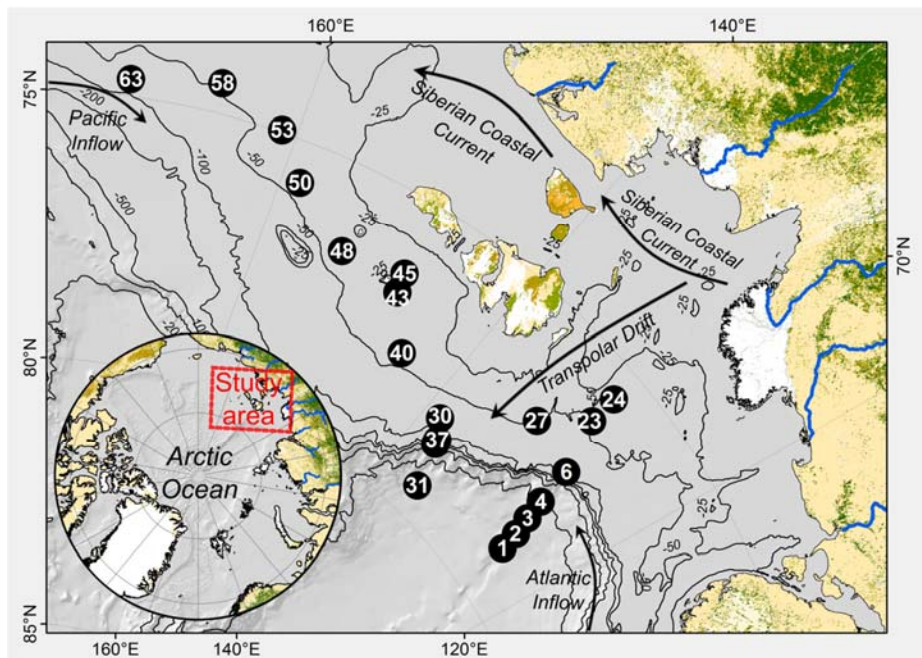
Table 3. Anaerobic rates of carbon mineralization by manganese, iron, and sulfate reduction

	Net Fe <sup>2+</sup> production	Net Mn <sup>2+</sup> production	C-equivalent Fe + Mn reduction	<sup>35</sup> S-sulfate reduction	C-equivalent total anaerobic mineralization	Oxygen uptake	% Fe + Mn reduction of total anaerobic	Percentage anaerobic C mineralization n of total	Percentage Fe and Mn mineralization n of total
	mmol m <sup>-1</sup> d <sup>-1</sup>						%		
Station 23	0.05	0.03	0.03	0.56	1.1	5.0	2.3	22.9	0.5
Station 30	0.02	0.04	0.03	0.05	0.1	2.6	21.9	4.4	1.0
Station 45	0.14	0.12	0.09	0.21	0.5	4.0	18.3	12.8	2.3
Station 53	0.15	0.09	0.08	0.14	0.4	4.5	23.7	7.8	1.8
Station 63	-	0.50	0.25	1.41	3.1	10.7	8.1	26.0	2.3

Table 4. Calculated carbon isotope composition of remineralized DIC and mass fractions of the marine and terrestrial endmembers and corresponding terrestrial carbon degradation rates based on <sup>35</sup>S-SRR and DIC flux

Station	Average δ <sup>13</sup> C <sub>DIC</sub> remineralized	Marine end member	Terrestrial end member	<sup>35</sup> S-SRR-based terrestrial degradation rate	DIC-based terrestrial degradation rate
	‰ vs. VPDB	Mass fraction		mmol m <sup>-2</sup> d <sup>-1</sup>	mmol m <sup>-2</sup> d <sup>-1</sup>
1	-35.8	0.0	1.0	0.13	0.11
4	-24.7	0.73	0.27	0.05	0.04
6	-25.1	0.65	0.35	0.01	0.03
23	-24.5	0.78	0.22	0.12	0.03
24	-24.7	0.73	0.27		0.06
27	-25.4	0.58	0.42	0.12	0.11
30	-28.5	0.00	1.00	0.05	0.13
Average Laptev Sea shelf	-25.6	0.53	0.47	0.08	0.07
40	-21.4	0.72	0.28	0.08	0.05
45	-22.2	0.63	0.37	0.08	0.14
48	-23.0	0.54	0.46	0.28	0.32
50	-24.0	0.43	0.57	0.77	0.57
53	-18.8	1.00	0.00	0.00	0.00
58	-22.6	0.59	0.41	0.42	0.53
63	-20.3	0.84	0.16	0.25	0.22
Average East Siberian Sea shelf	-21.8	0.68	0.32	0.27	0.26

Table 5. Regional estimates of sediment carbon mineralization in the outer Laptev and East Siberian shelf sea							
			Dissolved O <sub>2</sub> uptake	Upward DIC flux (anaerobic)	Terrestrial OC- derived DIC flux (anaerobic)	Marine OC- derived DIC flux (anaerobic)	Depth-integrated <sup>35</sup> S-SRR (C equivalent)
Outer Laptev Sea	Average	mmol m <sup>-2</sup> d <sup>-1</sup>	4.2	0.16	0.07	0.09	0.09
Outer East Siberian Sea	Average	mmol m <sup>-2</sup> d <sup>-1</sup>	7.2	0.73	0.26	0.47	0.34
Outer Laptev Sea	280,000 km <sup>2</sup>	Tg C y <sup>-1</sup>	5.2	0.20	0.09	0.11	0.11
Outer East Siberian Sea	340,000 km <sup>2</sup>	Tg C y <sup>-1</sup>	10.8	1.09	0.39	0.70	0.50
Total outer shelf area	620,000 km <sup>2</sup>	Tg C y <sup>-1</sup>	15.9	1.28	0.48	0.81	0.62
			<sup>35</sup> S-SRR- based terrestrial C degradation	<sup>35</sup> S-SRR- based marine C degradation	Total TEAP- based anaerobic OC degradation rate	Total TEAP- based anaerobic terrestrial OC degradation rate	Total TEAP- based anaerobic marine OC degradation rate
Outer Laptev Sea	Average	mmol m <sup>-2</sup> d <sup>-1</sup>	0.04	0.05	0.15	0.05	0.10
Outer East Siberian Sea	Average	mmol m <sup>-2</sup> d <sup>-1</sup>	0.13	0.21	0.42	0.16	0.26
Outer Laptev Sea	280,000 km <sup>2</sup>	Tg C y <sup>-1</sup>	0.05	0.07	0.18	0.06	0.12
Outer East Siberian Sea	340,000 km <sup>2</sup>	Tg C y <sup>-1</sup>	0.20	0.31	0.62	0.23	0.39
Total outer shelf area	620,000 km <sup>2</sup>	Tg C y <sup>-1</sup>	0.25	0.37	0.80	0.29	0.51

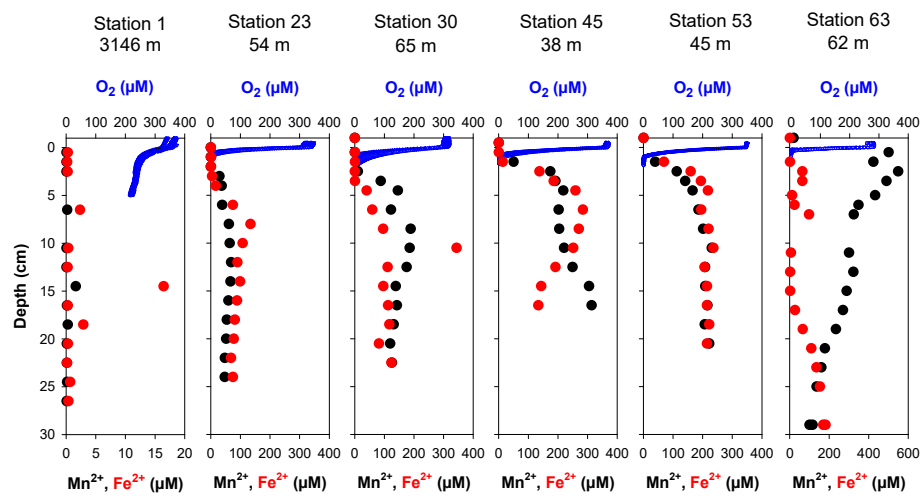


1177

1178 Fig. 1. Map of the Eastern Siberian Sea and slope and station locations.

1179

1180



1181

1182

1183

1184

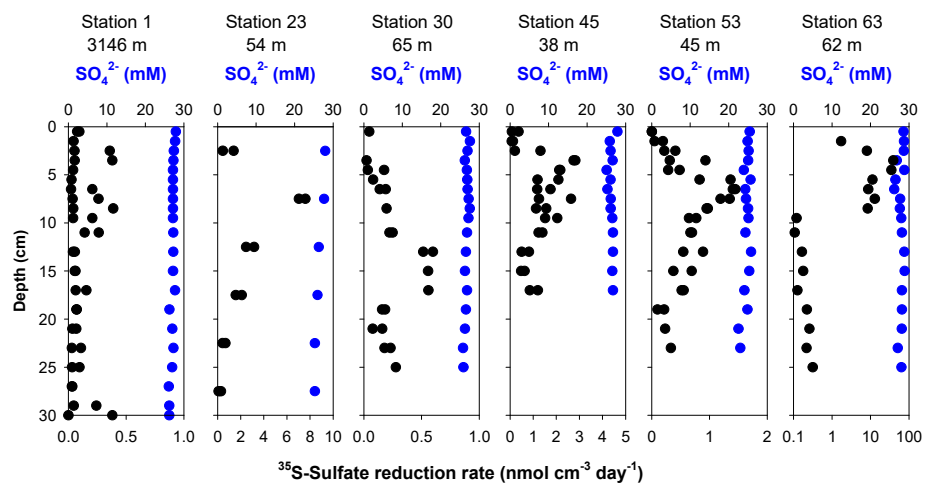
1185

1186

Fig. 2. Depth profiles of dissolved O<sub>2</sub>, Fe<sup>2+</sup>, and Mn<sup>2+</sup> at Stations 1, 23, 30, 45, 53, and 63. For microelectrode profiles, 4 replicates are shown for each station. Depth resolution of measurement for O<sub>2</sub> was 100 μm.

1187

1188



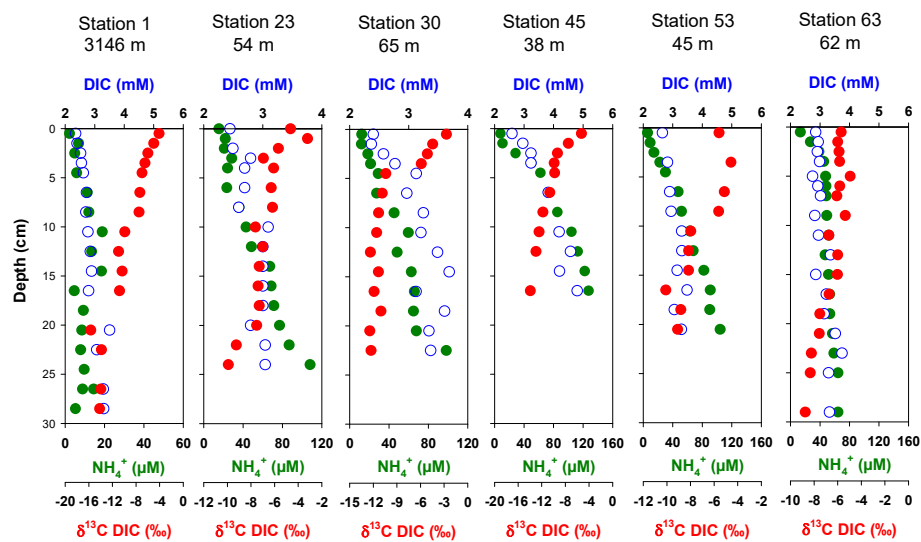
1189

1190 Fig. 3. Depth of profiles of  $^{35}\text{S}$ -sulfate reduction rates and porewater concentration of dissolved  
 1191 sulfate for Stations 1, 23, 30, 45, 53, and 63. A replicate incubation was conducted for each depth  
 1192 except for Station 63.

1193

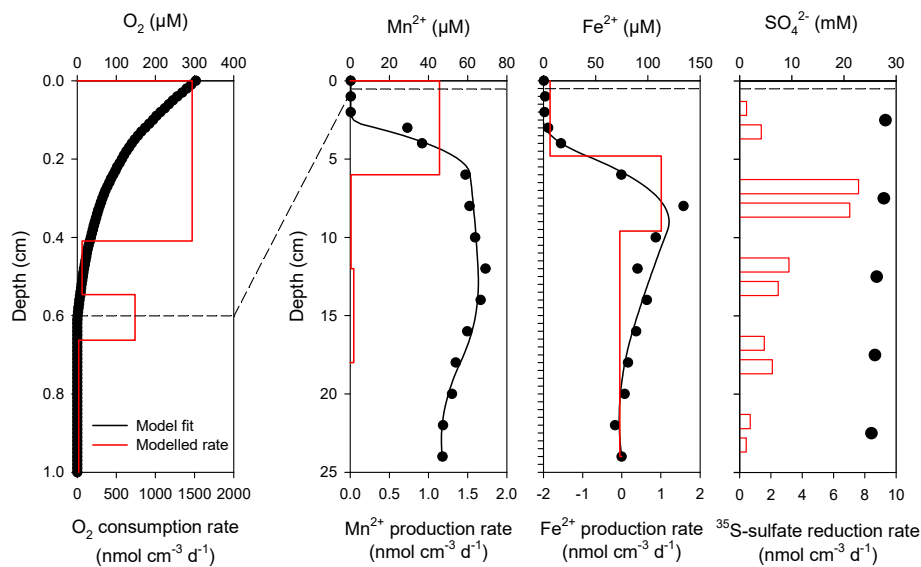


1194



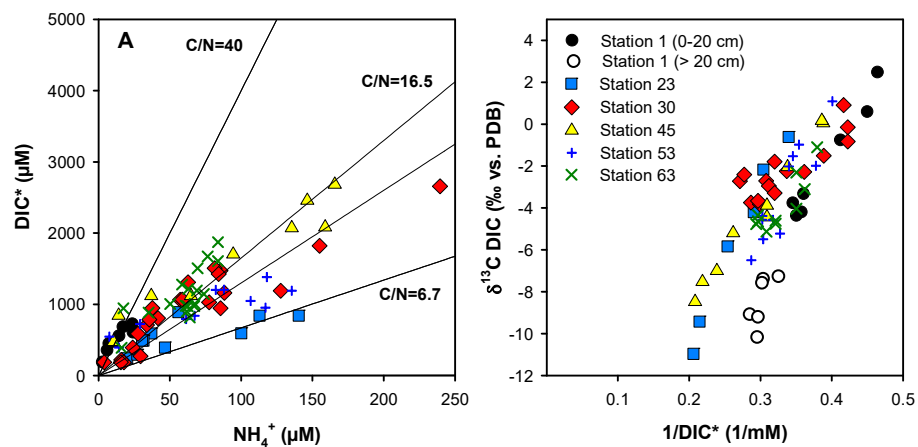
1195

1196 Fig. 4. Depth profiles of porewater dissolved inorganic carbon (DIC),  $\delta^{13}\text{C}$  DIC and porewater  $\text{NH}_4^+$  at  
1197 stations 1, 23, 30, 45, 53, and 63.



1198

1199



Field Code Changed

1200

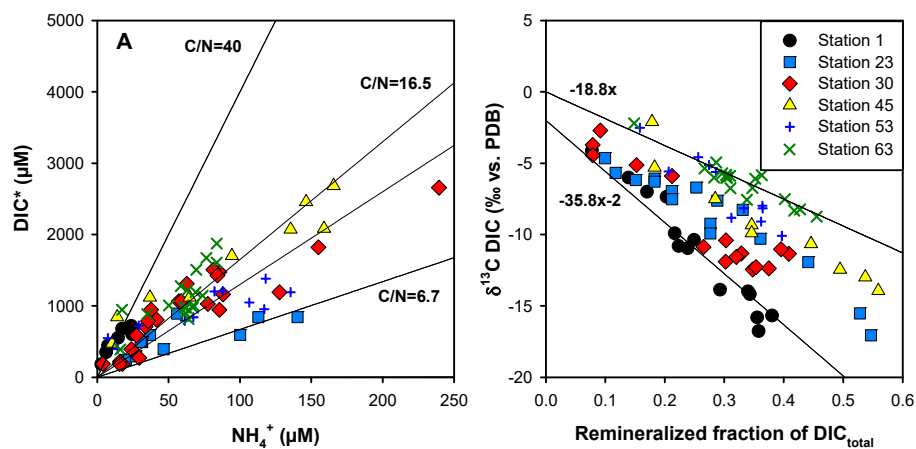
1201 Fig. 5

Formatted: Font: Times New Roman, 12 pt

1202 Fig. 5. Comparison of reaction rates of oxygen, manganese, iron, and sulfate reduction at Station  
1203 23. Note the different depth scale for the O<sub>2</sub> consumption rate. The dashed line marks the oxygen  
1204 penetration depth.

1205

1206



1207

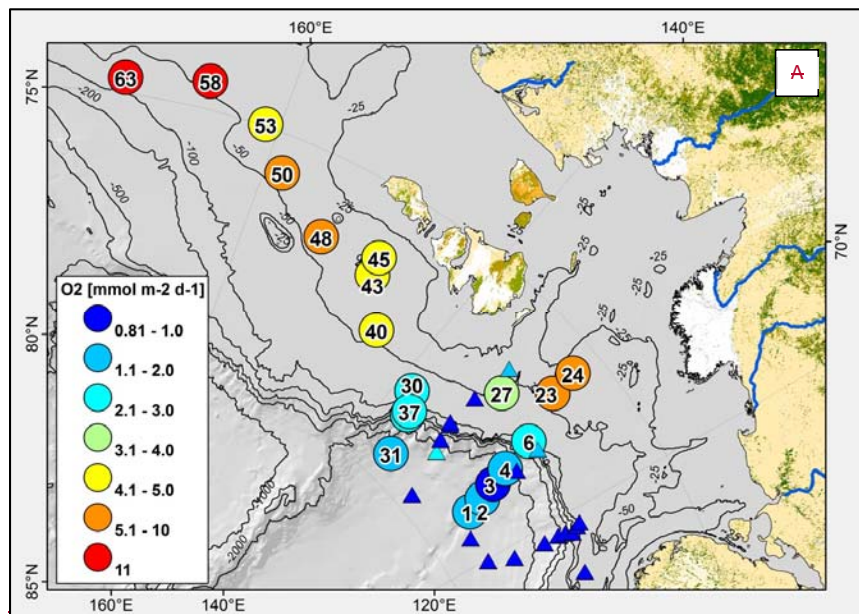
1208 Fig. 6. A: Crossplot of dissolved NH<sub>4</sub><sup>+</sup> and porewater DIC\* after correction for bottom water DIC  
1209 concentrations. The slopes of the regression lines for the individual stations are shown in Table 2. B:  
1210 Crossplot. A: Crossplot of dissolved NH<sub>4</sub><sup>+</sup> and porewater DIC\* after correction for bottom water DIC  
1211 concentrations. The slopes of the regression lines for the individual stations are shown in Table 2. B:  
1212 Keeling plot of the fraction of remineralized DIC calculated from a 2-endmember mixing model  
1213 versus δ<sup>13</sup>C DIC. The slope and y intercept of the regression for each station are shown in Table 3.

1214

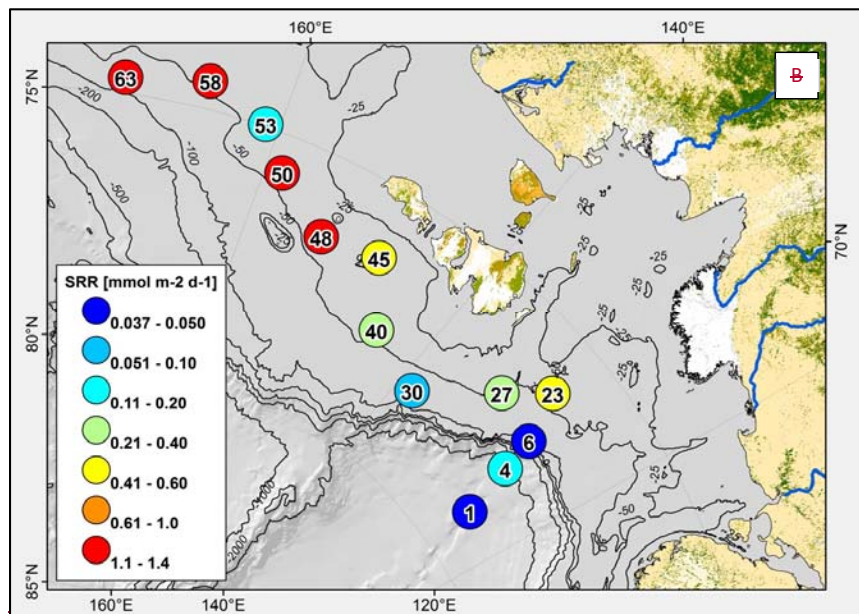
Formatted: Font: Times New Roman, 12 pt

Formatted: Font: +Body (Calibri), 11 pt

1215



1216



1217

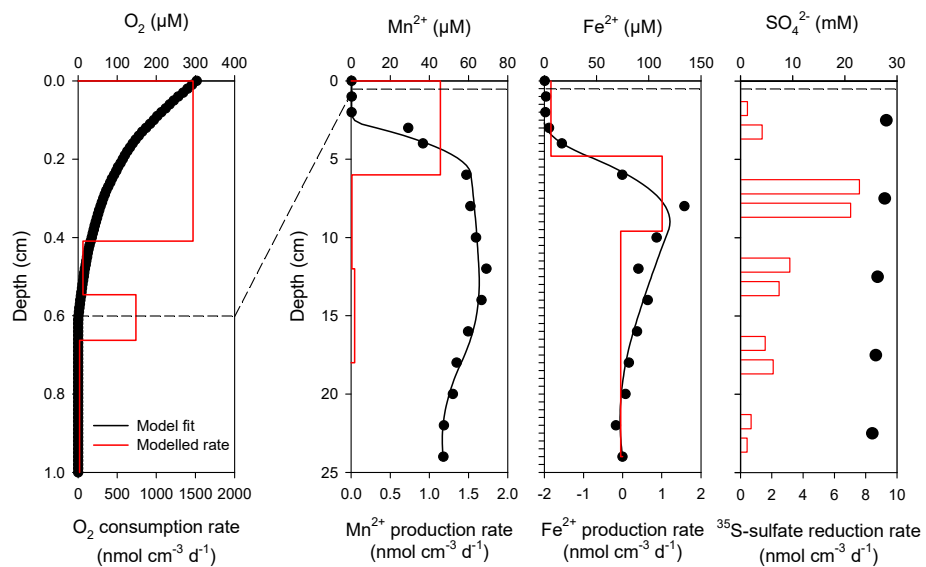
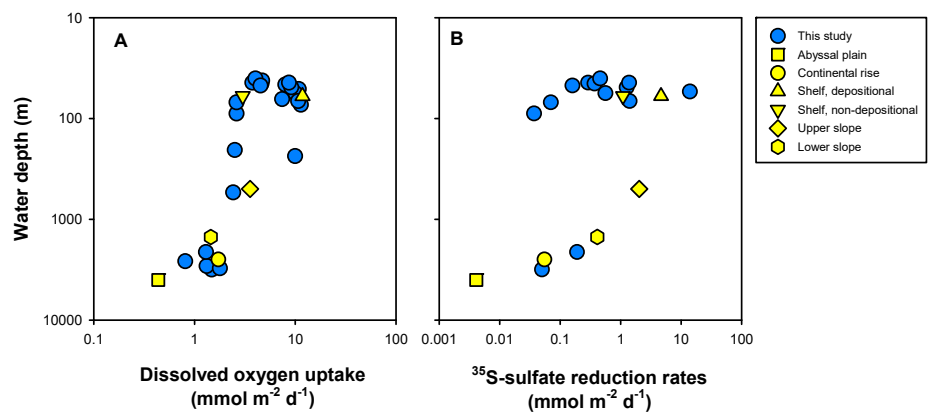


Fig. 7-A, B. Map 6. Comparison of field area and sampling stations showing oxygen uptake and reaction rates in panel A of oxygen, manganese, iron, and depth-integrated sulfate reduction rates in panel B at Station 23. Note the different depth scale for the  $O_2$  consumption rate. The dashed line marks the oxygen penetration depth.

1224  
1225  
1226  
1227  
  
1228

Formatted: Indent: First line: 1.27 cm



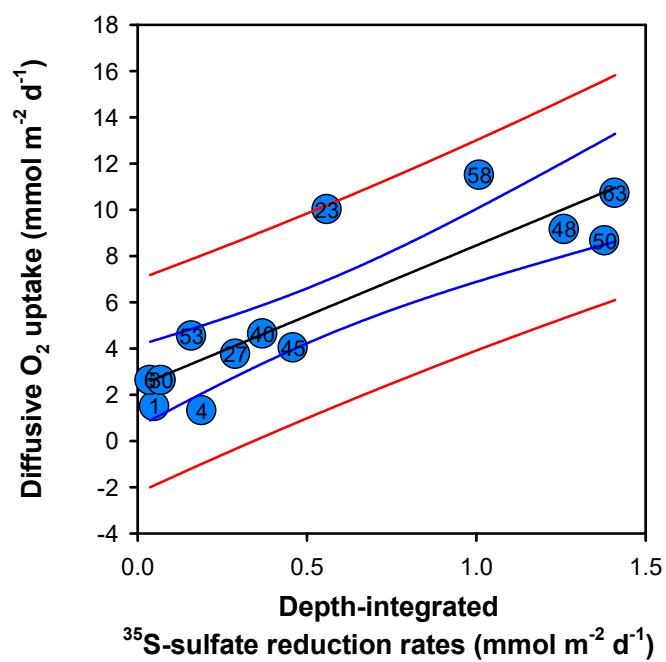


Fig. 7. Crossplot of diffusive oxygen uptake and integrated sulfate reduction rates. The black line is the linear regression and yielded a y-intercept of 2.1 mmol m<sup>-2</sup> d<sup>-1</sup> and a slope of  $6.1 \pm 0.1$ . Blue and red lines show the 95% and 99% confidence interval.

Field Code Changed

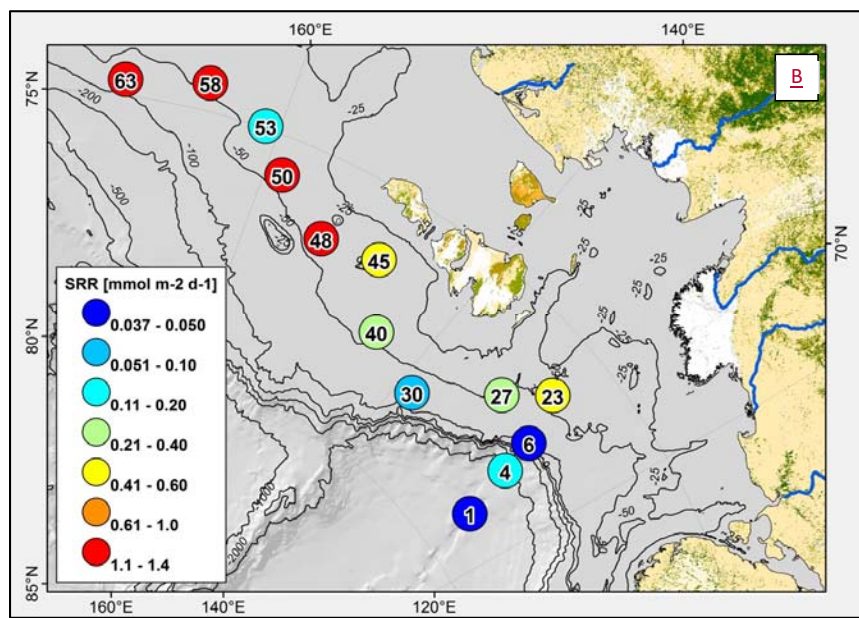
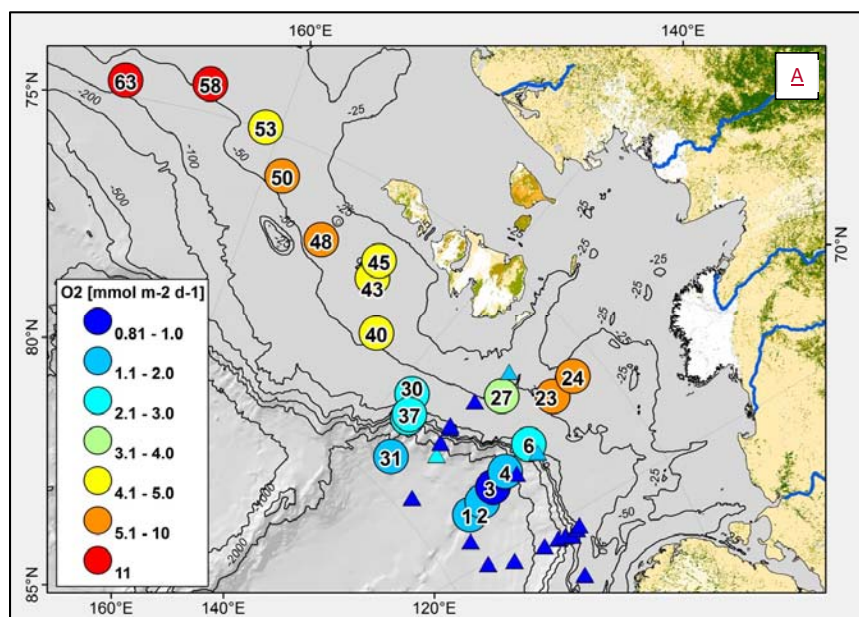


Fig. 8 A, B. Map of field area and sampling stations showing oxygen uptake rates in panel A and depth-integrated sulfate reduction rates in panel B.

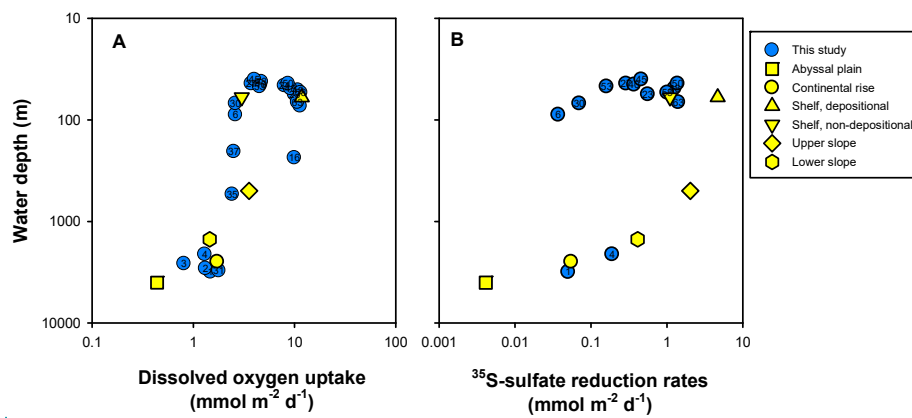
Formatted: Font: +Body (Calibri), 11 pt



1238

1239

8A



1240

1241

1242

1243

1244

**Fig. 9A.** Water depth variation of sediment oxygen uptake. **8B9B:** Water depth variation of integrated <sup>35</sup>S-sulfate reduction rates (0-30 cm sediment depth). For reference average rates of abyssal plain, continental rise, slope, and shelf sediments, deposition and non-depositional from Canfield et al. (2005).

Formatted: Indent: First line: 1.27 cm

Field Code Changed

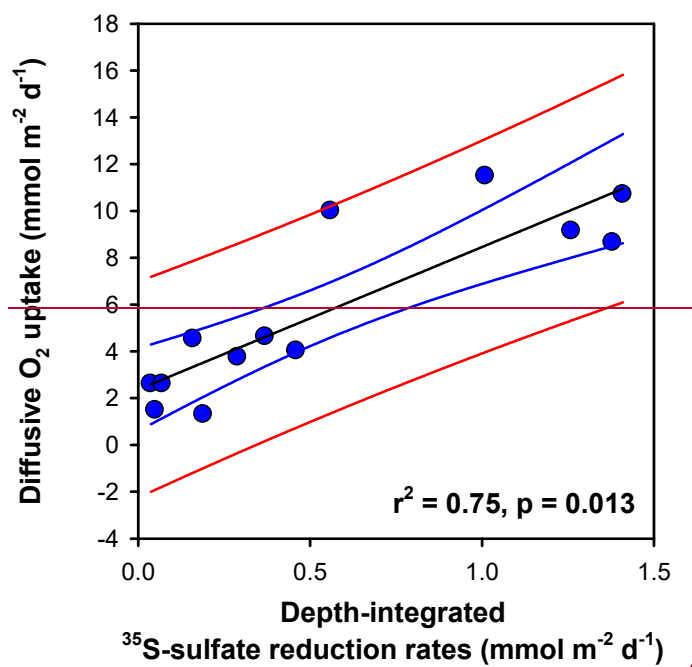


Fig. 9. Crossplot of diffusive oxygen uptake and integrated sulfate reduction rates. The black line is the linear regression and yielded a y intercept of 2.1 mmol m<sup>-2</sup> d<sup>-1</sup> and a slope of 5.55. Blue and red lines show the 95% and 99% confidence interval.

Formatted: Line spacing: 1.5 lines

Formatted: Font: Times New Roman, 12 pt, English (United States)

Formatted: Font: Times New Roman, 12 pt